

Article

Remotely Sensed Data, Morpho-Metric Analysis, and Integrated Method Approach for Flood Risk Assessment: Case Study of Wadi Al-Arish Landscape, Sinai, Egypt

Abdelrahman Khalifa ^{1,*} , Bashar Bashir ² , Abdullah Alsalman ², Sambit Prasanajit Naik ³ and Rosa Nappi ⁴ 

¹ Department of Geology, Faculty of Science, Al-Azhar University, Cairo 11884, Egypt

² Department of Civil Engineering, College of Engineering, King Saud University, P.O. Box 800, Riyadh 11421, Saudi Arabia; bbashir@ksu.edu.sa (B.B.); alsalman@ksu.edu.sa (A.A.)

³ Active Fault and Earthquake Hazard Mitigation Research Institute, Pukyong National University, Busan 48513, Republic of Korea; sambitnaik@pknu.ac.kr

⁴ Istituto Nazionale di Geofisica e Vulcanologia, Sezione di Napoli Osservatorio Vesuviano, Via Diocleziano 328, 80124 Napoli, Italy; rosa.nappi@ingv.it

* Correspondence: akhalifa@azhar.edu.eg

Abstract: Evaluating and predicting the occurrence and spatial remarks of climate and rainfall-related destructive hazards is a big challenge. Periodically, Sinai Peninsula is suffering from natural risks that enthruse researchers to provide the area more attention and scientific investigation. Extracted information from the morpho-metric indices aids in understanding the flood potentiality over various sizes of drainage catchments. In this work, the morpho-metric analysis has been used in order to model the relative signals of flood vulnerability of 16 catchments in northern Sinai. The geospatial technique has been applied to process the digital elevation models (DEMs) in order to produce different analysis maps. Basic geometries, in addition to several morpho-metric indices, were extracted and analyzed by investigating the digital elevation models. Three different effective methods were applied separately to build up three models of flood susceptibility behaviors. Finally, two flood susceptibility signals were defined: the integration method and accurate pixel level conditions models. The integrated method analysis indicates that the western half of the study landscape, including catchments (12, 13, and 14), presents high levels of flood susceptibility in addition to catchment 9 in the eastern half, whereas the other catchments were found to provide moderate levels. The integrated flood susceptibility final map overlaid one of the most effective topographic indices (topographic position index, TPI). The integrated results aided in understanding the link of the general catchments morphometry to the in situ topography for mapping the different flood susceptibility locations over the entire study landscape. Therefore, this can be used for investigating the surface-specific reduction strategy against the impacts of flood hazards in the proposed landscape.

Keywords: flood hazards; morphometric analysis; integrated method; topographic analysis; Wadi Al-Arish; northern Sinai; Egypt



Citation: Khalifa, A.; Bashir, B.; Alsalman, A.; Naik, S.P.; Nappi, R. Remotely Sensed Data, Morpho-Metric Analysis, and Integrated Method Approach for Flood Risk Assessment: Case Study of Wadi Al-Arish Landscape, Sinai, Egypt. *Water* **2023**, *15*, 1797. <https://doi.org/10.3390/w15091797>

Academic Editor: Achim A. Beylich

Received: 26 March 2023

Revised: 4 May 2023

Accepted: 5 May 2023

Published: 8 May 2023



Copyright: © 2023 by the authors. Licensee MDPI, Basel, Switzerland. This article is an open access article distributed under the terms and conditions of the Creative Commons Attribution (CC BY) license (<https://creativecommons.org/licenses/by/4.0/>).

1. Introduction

Globally, hazards that are driven by flooding are big obstacles to strategic development plans, causing numerous deaths and dreadful damages [1–3]. Due to the dramatic acceleration in flood hazard impacts during the last decades, numerous flash events have been discussed and assessed in different localities by different methods [4–9]. In Europe, significant scenarios and models had been presented to recognize changes in flood risks and hydrological behavior [10]. In Greece, geological and geomorphological parameters were applied to map a flood risk assessment model for some urban regions [8]. In Asia, flash floods are investigated and assessed using the most modern methods and applications. For example, a GIS technique was developed to assess the flood risk for the Makkah

metropolitan region in Saudi Arabia utilizing the most advanced and detailed datasets [11]. In Pakistan, floods, groundwater characteristics, and their socio-economic impacts on the country were commonly discussed by many authors [12,13]. In addition, modern techniques such as geographic information systems were applied to estimate and evaluate the total quantity of water bodies of the Peshawar basin [14]. Regarding Africa, particularly in Egypt, flood risk signatures between the El-Qussier and Marsa-Alam coastal region along the western coast of the Red Sea were investigated and preliminary evaluated [3]. Regarding impacts of flood hazards and rainfall storms on geomorphic changes, analogue and numerical significant works were discussed and presented [15–17]. For example, Ref. [15] discussed the geomorphic variance including deposition and erosion produced by huge floods. The flood hazards above were investigated and evaluated using various types of data and techniques. Therefore, collecting and analyzing high-resolution spatial data in addition to building reliable and comprehensive models aid in designing an effective mitigation plan against these natural hazards. The evaluation of relative activity signals, uplifting, drainage systems, and catchments analysis of active folds, faults, and uplifting rates can be effectively recognized through a deeper understanding of the tectonic geomorphology applications [17]. Studying and calculating morpho-metric parameters, including a catchment total area (A), a catchment perimeter (P), the total length of a catchment (Lc), average elevations of catchments, stream orders (Su), total stream lengths (Lu), stream numbers (Nu), bifurcation ratio (Rb), stream frequency (Fs), form factor (F), drainage density (Dd), texture ratio (Rt), infiltration number (If), catchment relief (Hr), ruggedness number (Rn), and elevation ratio (Rr) are very useful and effective keys to evaluate to attempt to mitigate the impact of recent flash flood hazards.

Regarding the natural hazards response side, communities are not prepared enough to face the negative effects of flood hazards representing a great challenge to the governments and hazards management institutions [18,19]. Despite of huge efforts of most hazards-prone countries, it may take a long time to recover from the loss of lives and infrastructure [20]. One of the most effective warning methods is hazard monitoring, which represents the first step in reducing the serious damages of potential flash floods. Understanding flood vulnerabilities is not only a vital strategy to face flood hazards, but also dealing with capacities and precipitation may help in implementing appropriate signals of flood hazards reduction [20]. Flood hazard communication plays an important role in the hazard perception of people by transferring information about oncoming flood hazards and improving their knowledge about the preventive measures [21]. In addition, many studies claim that these communication tools may be affected by the sources of the hazards [22–24].

The Sinai landscape is a distinct triangular landform connecting Asian and African continents. It is surveyed as a region between $27^{\circ}45'–29^{\circ}55'$ (latitudes) and $32^{\circ}40'–34^{\circ}50'$ (longitudes). It is fully surrounded by the Aqaba Gulf, the Suez Gulf, and the Mediterranean Sea from the east, west, and north, respectively (Figure 1). This study deals with the Wadi Al-Arish landscape, which accounts for the largest water system catchment in the Sinai Peninsula, occupying a major part of Egypt and a small part of Palestine country. Recently, the Egyptian government provided the Sinai Peninsula more attention for study and development. Huge construction and economic projects were initiated to start the preliminary steps of developing a plan; the government motivated and supported researchers to focus on finding solutions to help reduce the impact of hazards and environmental changes. This paper is aiming to (a) present a new model by quantifying several morpho-metric indices to examine the flash flood signals, (b) investigate anomalies in order to produce a new scheme of flood hazard assessment, (c) and expand our knowledge and understanding of the morphological behaviors under the impact of the flash flood risks.

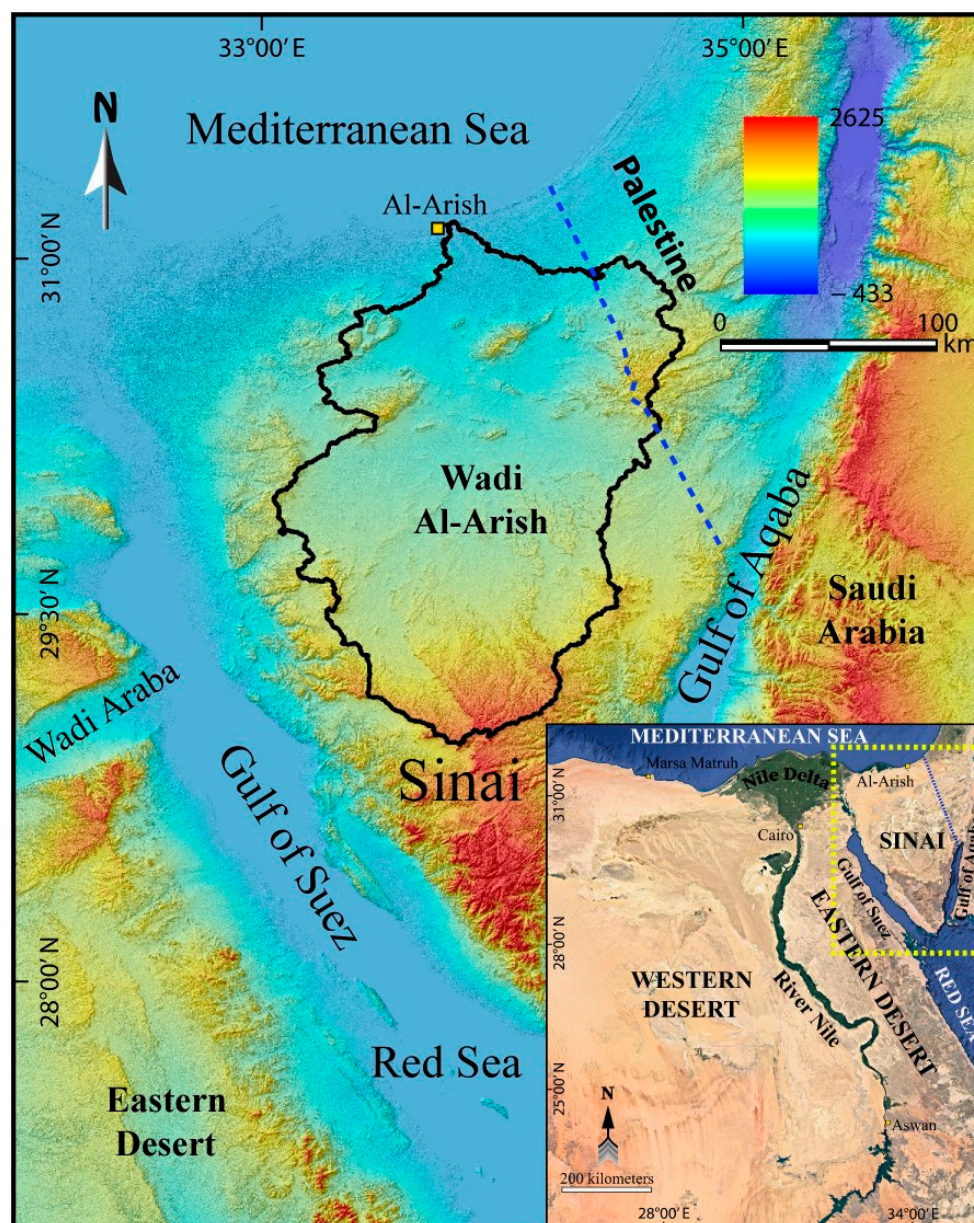


Figure 1. Hill-shade image (data from SRTM-30; <https://earthexplorer.usgs.gov/>, accessed on 23 September 2022) of Northern Red Sea presenting Sinai Peninsula, Suez Gulf, and Aqaba Gulf. Blue dashed thin line states the political boarder. The index map and box with yellow dashed thick lines show location of the study landscape.

2. Study Landscape

The Wadi Al-Arish catchment landscape lies in the northern part of Egypt occupying most of the Sinai Peninsula (Figure 1). The Wadi Al-Arish catchment is recognized between $29^{\circ}00'$ and $31^{\circ}00'$ north and $33^{\circ}05'$ and $34^{\circ}45'$ east, providing an area of $\sim 23,300 \text{ km}^2$, which represents $\sim 36\%$ of the total space of the Sinai area. Most water tributaries come from the Sinai Peninsula ($\sim 91\%$), and a few run from the adjoining El-Naqb Desert [25–27]. The Wadi Al-Arish catchment drains the central Sinai highlands and its upstream tributaries drain from El-Teeh and El-Egma plateaus [26]. Climatologically, The climatic characteristics of the Sinai landform provide important factors in developing Sinai's ecological conditions over the entire Peninsula [27]. Although Sinai is known as an arid region, it is characterized by frequent flash floods that occur with various magnitudes [25,27,28]. In a recent flood (January 2010), around 12 people were affected and many properties were damaged [25,29].

This was followed by another major flood in March 2014, continuing for 20 h and causing huge damages [29]. The cumulative data from the temperature and rainfall state that Wadi Al-Arish is a big dry catchment, where the average temperature in summer ranges from 25 °C to 43 °C. The recorded temperature during the winter varies between 10 °C and 3 °C. The available precipitation data of Wadi Al-Arish were extracted and processed from the data Access viewer NASA Power site (<https://power.larc.nasa.gov/data-access-viewer/>, accessed on 20 February 2022) between 2013 and 2021 (Figure 2). The lowest mean annual rainfall was recorded for 2006, while the highest quantities were observed for 2018 (Figure 2).

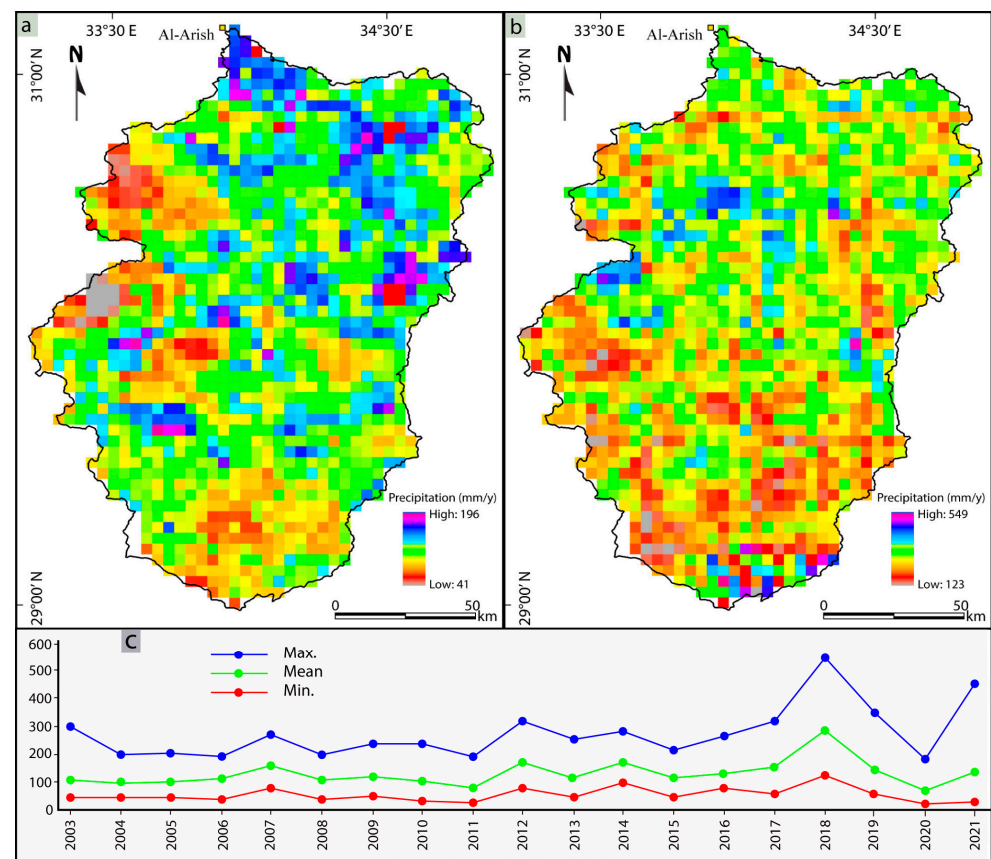


Figure 2. (a) precipitation pattern of 2006; (b) precipitation pattern of 2018; and (c) precipitation rainfall from 2003 to 2021.

The lithology of the Sinai has been recognized and mapped by several researchers [30–33]. The lithological distribution of Wadi Al-Arish was remodified due to the recent literature and Conoco geological maps of Egypt [30] (Figure 3). The lithological units and formations in Wadi Al-Arish range from Pre-Cambrian units to Quaternary deposits. The recorded Middle Jurassic age is represented by Safa Formation. Masajed Formation was deposited after representing the middle–upper Jurassic age. The Risain’Aneiza Formation was mapped in the study area recording the lower Cretaceous age, while the upper Cretaceous age is represented by Matulla and Suder Formations, respectively. Regarding the Tertiary age, the Paleocene provides deposits that are recognized as Esna Formation, while the Thebes group was observed and mapped in the study area recording lower Eocene. Finally, the Plio-Pleistocene and Quaternary ages were recorded, covering the majority of the studied landscape. More details about the units and formations of the current study landscape are presented in Figure 3.

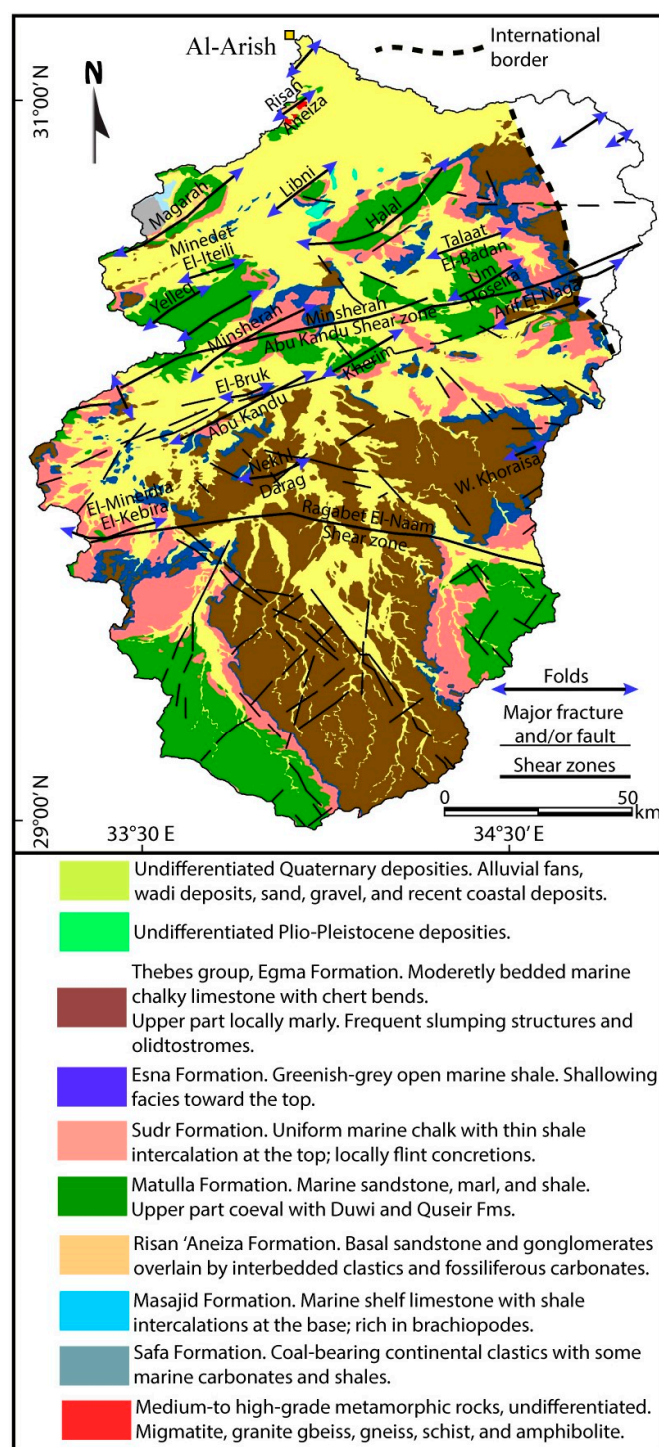


Figure 3. Detailed geological map of Wadi Al-Arish, Sinai modified from Reference [30].

Structurally, the Wadi Al-Arish catchment is highly deformed by different structural features (Figure 3). Two major shear zones were recognized, they are Ragabet El-Naam and Minsherah Abu kandu Shear zones crossing Wadi Al-Arish in an E–W and NE–SW trend, respectively (Figure 3). Fractures that are observed in the study catchment provide clues to two different fracture systems including NE–ENE and NW–WNW trends. Therefore, authors in References [27,34] state that these recorded fractures play a significant role in the trending and incision rate of the majority of the proposed drainage systems. For example, the southern part of the Wadi Al-Arish catchment presents a compatibility relation between the main courses of the water systems and the majority of the fractures trending.

Additionally, Wadi Al-Arish records many anticlinal folds. They are distributed between the northern tip of Wadi Al-Arish and the Ragabet El-Naam Shearing, providing mostly NE–SW trends (Figure 3) [34].

Morphologically, Wadi Al-Arish provides several morphological signatures due to the effect of tectonics and different rock types [27]. The study by [26] states that the morphological differences, including variations in elevations and positions, are the direct cause of the differences in climatic conditions during the same season. Regarding topography impacts, the surface elevation of the Wadi Al-Arish landscape recorded its highest values in the south part as 1632 m a.s.l., while the lowest topographic values were observed in the northern parts of the studied region. Therefore, we can simply describe the general surface elevation of Wadi Al-Arish as a major landscape with high elevation at the south that gradually decreases towards the Mediterranean Sea (Figure 4a). The slope map is derived from the DEM using the ArcGIS 10.4 software. The slope information was analyzed, providing values between 0 and 57° (Figure 4b). Usually, the height slope values are encountered along the basins upstream, while the lowest values indicate the basin outlets [27]. Therefore, the variations in the general slopes of Wadi Al-Arish are controlled by topographical variation signals.

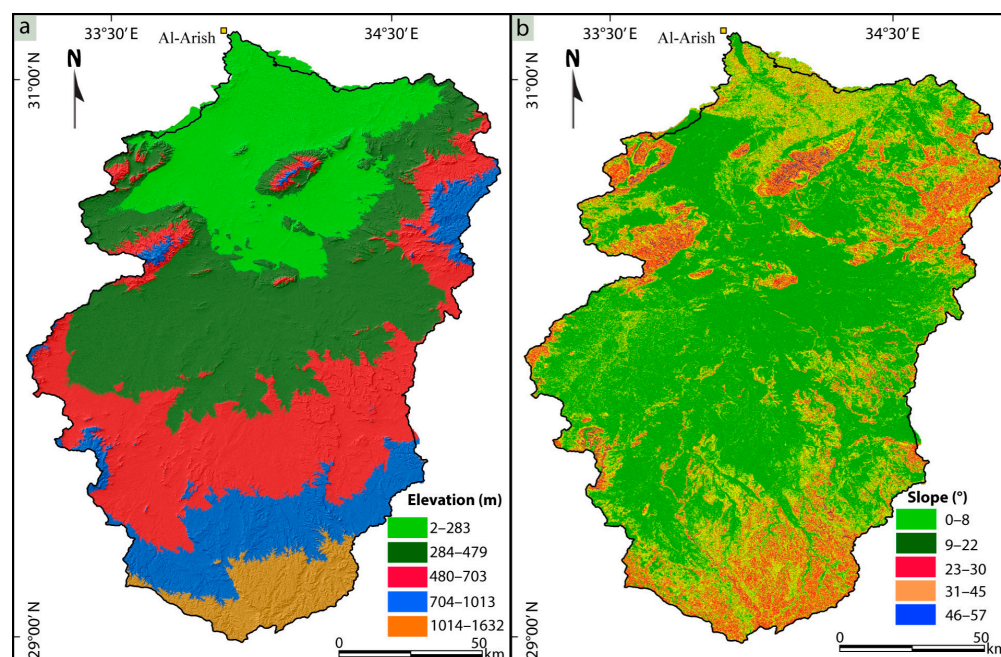


Figure 4. (a) Digital elevation model and (b) slope maps showing the general elevations and slopes of Wadi Al-Arish region.

3. Materials and Methodology

Different vector and raster datasets were collected and applied in this work. Two geological maps of Conoco, 1987 (Northern Sinai and Southern Sinai sheets), were used to distinguish the lithological units and formations and extract the different structural elements of the study landscape. Remotely sensed data of the digital raw form of the DEMs (Shuttle Radar Topography Mission, SRTM) data with 30 m resolution were acquired from the USGS website, <https://earthexplorer.usgs.gov/>, accessed on 23 September 2022. The topographical maps (Scale: 1:100,000), in addition to DEMs data, were combined and rectified to extract the different topographical data (e.g., elevation and hill-shade maps).

The methodology runs through various steps and processes as shown in Figure 5. The pre-processing section deals mainly with the raw data of the DEMs. Rectifications and data corrections were the first step for preparing data extraction. Filling correction step, raster flow direction, raster flow accumulation, snap pour step, stream order, and stream feature step were run from the hydrology toolbox to extract the drainage systems and

different watersheds delineation. In this study, the Wadi Al-Arish landscape was classified into 16 catchment utilizations of greater than the fourth order (Figure 6a,b) using the hydrology tools in ArcGIS 10.4 software. The derived values of the catchments' geometric characteristics, including catchment total area, catchment perimeter, catchment length, and catchment average elevation show that: the biggest area is recorded for catchment 14, while the highest extracted values of perimeter was accounted for in catchment 12. The extraction geometries also show that the longest catchment length was recorded in the southern site of the study landscape for catchment 11. Catchment 5, located at the northern part of the study landscape, provides the lowest value of the catchment area and perimeter as 81.78 km² and 46.12 km, respectively. The lowest catchment length value was observed for catchment 5. The results for all catchments are tabulated in Table 1. The processing section is mainly covering the idea of an integrated methods approach. In this study, the comparative quantitative analysis between watershed level, El-Shamy, and ranked techniques was tested and used to figure out the results compatibility levels through three different quantitative methods. The final processing step aimed to merge the final integrated methods of the flood susceptibility map with two effective surface and witness flow-affecting morphology indices (TPI and TWI, Table 2). This combination process aims to recognize comparative flood risk signals of different catchments and classify accurately the different spots within the catchments illustrating higher flash flood susceptibility levels. This process runs based on the conversion of all data to the raster format through the same (WGS 1984; UTM 37 N zone) projection.

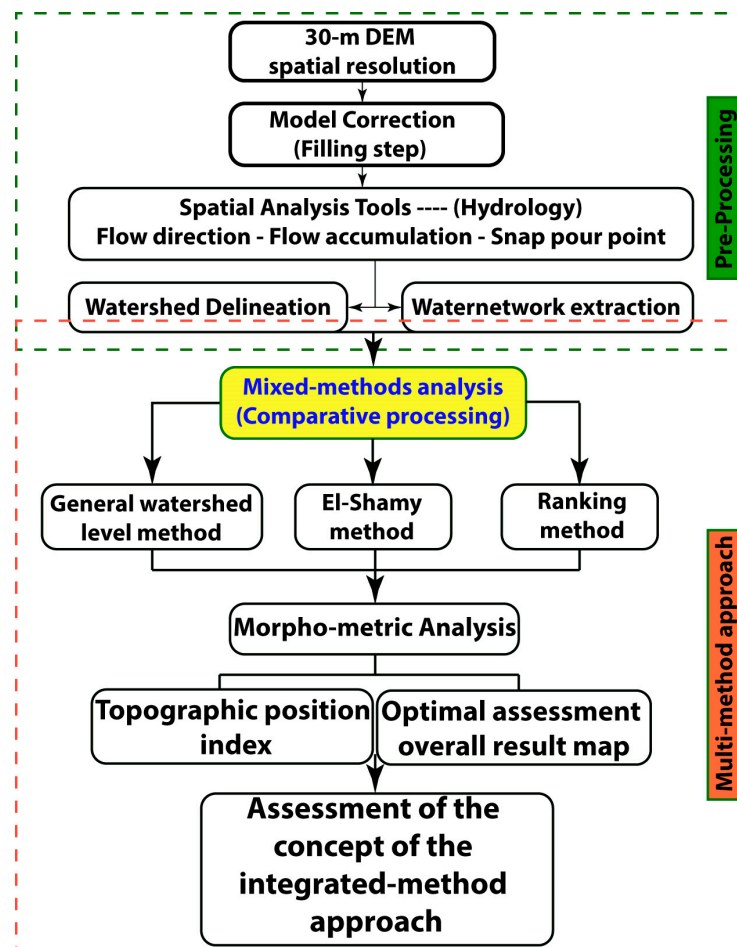


Figure 5. Flowchart presenting the applied methodology.

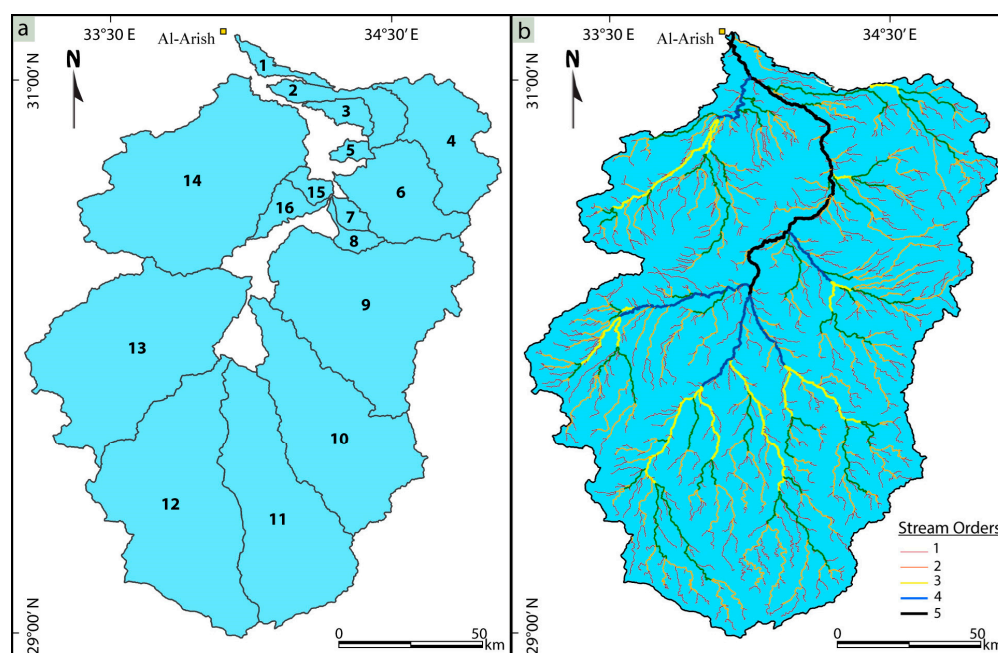


Figure 6. (a) Catchments (1–16) and (b) stream orders of the study landscape.

Table 1. Basic geometric attributes of the proposed catchments.

Catchments	Area	Perimeter	Length	Elevation	Elevation
	(km ²) (A)	(km) (P)	(km) (Lu)	(m) Max (H)	(m) Min (h)
C1	142.2	100.74	41.1	149	04
C2	402.45	149.65	61.2	463	27
C3	164.18	76.38	29.6	341	93
C4	1067.01	201.15	34.5	1023	151
C5	81.78	46.12	14	460	162
C6	1000.85	169.06	50.9	1030	172
C7	104.69	46.42	19	461	189
C8	124.25	70.3	28.2	656	190
C9	2888.03	283.34	62.2	999	231
C10	2347.29	277	95.2	1198	305
C11	2454.98	273.13	104	1630	372
C12	3237.79	314.27	96.9	1603	372
C13	3111.62	301.95	80.5	1050	288
C14	3351.79	301.25	78.3	1077	45
C15	220.16	92.87	23.7	897	189
C16	119.73	54.1	17.4	908	178

3.1. Integrated Method Analysis

3.1.1. General Watershed Level Method

In our first method, we aimed to understand differences in relative flash flood hazards of the classified catchments by examining values that come from basic geometries and morpho-metric indices. For a consistent analysis, the calculated values of the selected morpho-metric indices of every single catchment are subsequently classified into an adapted common evaluation scale of 1–3 as low, moderate, and high flood susceptibilities. Regarding the nature of the range within a single morpho-metric index (– or + relation about flash flood level scale), a new averaged value is stated for each index of all the catchments. Lastly, a cumulative value digit is extracted in order to assign the flood vulnerability levels for every single catchment in a final flood susceptibility map.

3.1.2. El-Shamy Method

The concept of this method is mainly applied to just three major morpho-metric indices: drainage density index, stream frequency index, and bifurcation ratio index, presenting three different levels of flood hazard degrees (low, moderate, and high). To evaluate the flood hazard levels of the Wadi Al-Arish landscape, the approach developed by the author in Ref. [35] is applied. This method uses two diagrams for measuring effectively the hazardous degree of the different landscapes. It states the relations between the bifurcation ratio index against stream frequency and drainage density indices for every single proposed catchment. Each diagram presents three zones: zone 1 (A) is covering catchments that are characterized by high conditions of ground recharge and low vulnerability degree for flash flood events; zone 2 (B) indicates areas with high potentiality conditions for flash floods and providing low remakes of groundwater recharge; and finally, zone 3 (C) provides intermediate degrees for both floods and groundwater recharge.

3.1.3. Ranked Method

Regarding this method, Authors in Ref. [36] recognized and developed an effective method to evaluate the flood hazard levels of landscape catchments [37,38]. Scaling flood risk into 6 levels is the core analysis of this method. The levels are set to all calculated morpho-metric indices for all catchments of the study landscape. Fold levels present numbers 1, 2, 3, 4, and 5, indicating low, moderate, high, very high, and extreme flood risks, respectively [36,38]. To calculate the actual risk levels for a catchment using the ranked method, a geometric relationship developed by the author in Ref. [39] is required. The following geometric relations are set for the indices that provide a directly proportional relationship and an inversely proportional relationship, respectively.

$$\text{Flood risk level} = [4 \times (X - X_{\min}) / X_{\max} - X_{\min}] + 1 \quad (1)$$

$$\text{Flood risk level} = [4 \times (X - X_{\max}) / X_{\min} - X_{\max}] + 1 \quad (2)$$

where X indicates values of the morpho-metric index for every single catchment, while X_{\max} and X_{\min} parameters define the maximum values and minimum values of the calculated index through the proposed all catchments. For a consistent strategy of the methods applied in this study, the flash flood evaluation scale was modified and reset into 3 risk levels, providing number 1 (low level), number 2 (moderate level), and number 3 (high level). Thus, the calculations of this method are applied through the following modified geometric proportional relationship as direct and inverse, respectively.

$$\text{Flood risk level} = [2 \times (X - X_{\min}) / X_{\max} - X_{\min}] + 1 \quad (3)$$

$$\text{Flood risk level} = [2 \times (X - X_{\max}) / X_{\min} - X_{\max}] + 1 \quad (4)$$

3.2. Morpho-Metric Analysis

Quantitative values of the morpho-metric indices have long been calculated to examine the elementary flood vulnerability signals and understand the origin and nature of the drainage catchments [3,40–45]. Based on the considerable influence of the morph-metric behaviors on the various hydrological impacts of the catchments (Figure 7), many studies have discussed how drainage catchment morphometry acts as a significant key in the intensity and occurrence of flood events [3,45,46].

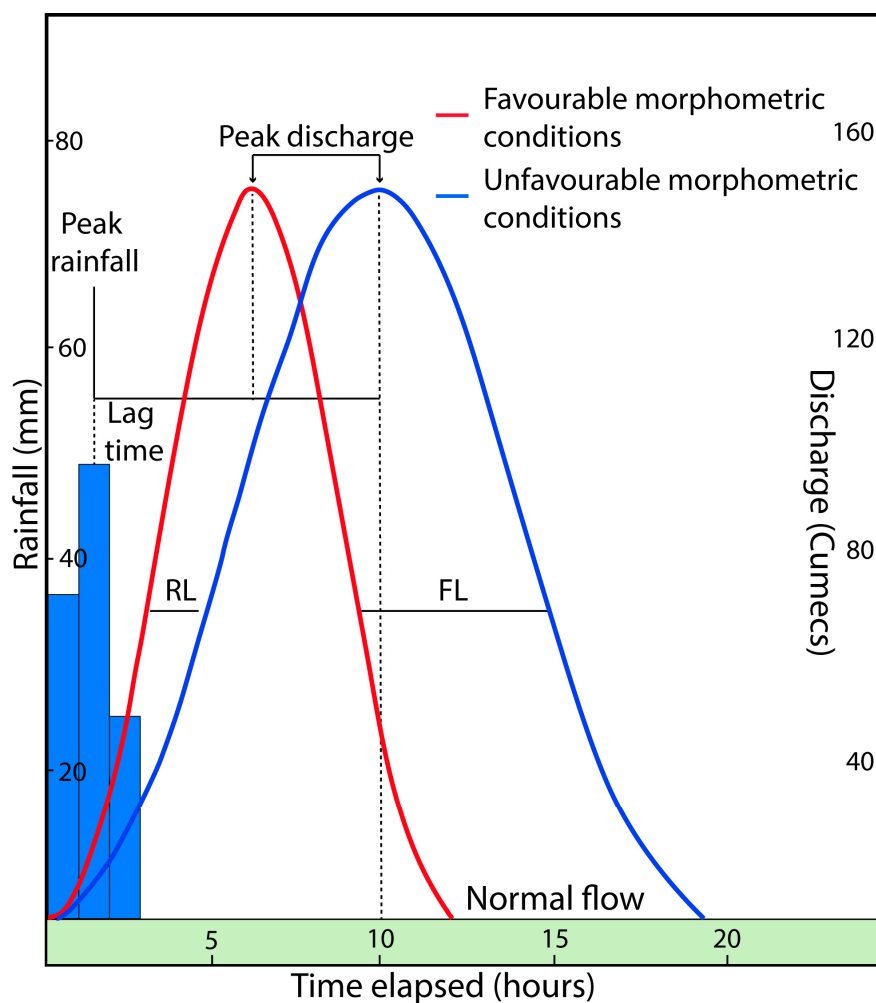


Figure 7. Hydrograph chart presenting the impact of drainage catchment morphometry regarding peak discharges; FL: falling limb; RL: rising limb; modified after Ref. [45].

Table 2. Morpho-metric and topographic indices for the present study.

Index	Mathematical Equation	References
Catchment Area (A , km^2)	A measures the total area from drainage divide to catchment outlet edge	[17,47]
Perimeter (P , km)	P measures the total catchment length	[3,47]
Catchment length (L_c , km)	L_c indicates the maximum length of the catchment is defined parallel to the main catchment course	[47]
Stream number (N_u)	$N_u = N_1 + N_2 + N_3 + N_4 + \dots + N_n$	[48]
Stream length (L_u)	$L_u = L_1 + L_2 + L_3 + L_4 + \dots + L_n$	[48]
Stream order (S_u)	Hierarchical rank	[49]
Bifurcation ratio (R_b)	$R_b = N_u / N_{u+1}$, where streams number values of any calculated order, and N_{u+1} represents the stream number value for the next higher order	[47]
Stream frequency (F_s)	$F_s = N_u / A$, where N_u provides the total number of all stream orders and, A measures the catchment total area	[46]
Form factor (F)	$F = A / L_c^2$, where A measures the catchment total area, and L_c^2 represents the squared catchment length	[43]

Table 2. Cont.

Index	Mathematical Equation	References
Texture ratio (Rt)	$Rt = Nu/P$, where Nu provides the total number of all stream orders, and P measures the exact catchment perimeter	[50]
Drainage density (Dd)	$Dd = Lu/A$, where Lu measures the catchments segments total length, and A is providing the catchment total area	[48]
Infiltration number (If)	$If = Fs/Dd$, where Fs represents the average stream frequency, and Dd presents drainage density	[51]
Catchment relief (Hr , m)	$Hr = Hmax - Hmin$, where $Hmax$ and $Hmin$ indicate the highest and lowest elevation points of the given catchment, respectively	[47]
Ruggedness number (Rn)	$Rn = Dd \times (Hr/1000)$, where Dd indicates the drainage density, and Hr presents the catchment topography	[52]
Elevation–relief ratio (Rr)	$Rr = Hr/L$, where Hr measures the catchment topography, and L provides the catchment total length	[48]
Topographic position Index (TPI)	$TPI = M0 - \sum_{n=0}^n (Mn/n)$, where $M0$ provides elevation of the model point under evaluation, Mn measures the elevation of the grid, and n measures the total number of surrounding points applied in the evaluation processes	[53]

4. Results and Discussion

4.1. Morpho-Metric Analysis

In this study, the basic morpho-metric indices were investigated and extracted. In the next subtitles, the calculated results of the quantitative analysis of the morpho-metric indices, average calculated values, topographic position analysis, and flood susceptibility levels are analyzed and discussed.

4.1.1. Stream Number Index (Nu)

In general, drainage watersheds that provide dense stream numbers, present a high level of runoff conditions and reach a high peak flow during heavy rainfall events [45,54,55]. Stream number results provide the highest value for the biggest catchment (C14), while the lowest value was observed for catchment 5, providing the least runoff capacity conditions (Table 1 and Figure 8).

4.1.2. Stream Order Index (Su)

The stream order (Su) index is one of the most important indexes of hydro-geomorphology to measure and examine the size of the catchments water paths. It is used to present a rank classification of the streams and rivers [40]. In the current study, catchments 4, 6, 9, 10, 11, 12, 13, and 14 provide the highest order of streams (VI), whereas catchments 2, 3, 5, 7, and 8 record IV orders as height orders (Table 3). Generally, high stream orders reflect the existence of large streams and rivers in the catchments fed by various small rivers and streams presenting high possibilities of flow velocities and water discharge based on the studied relief characteristics [45].

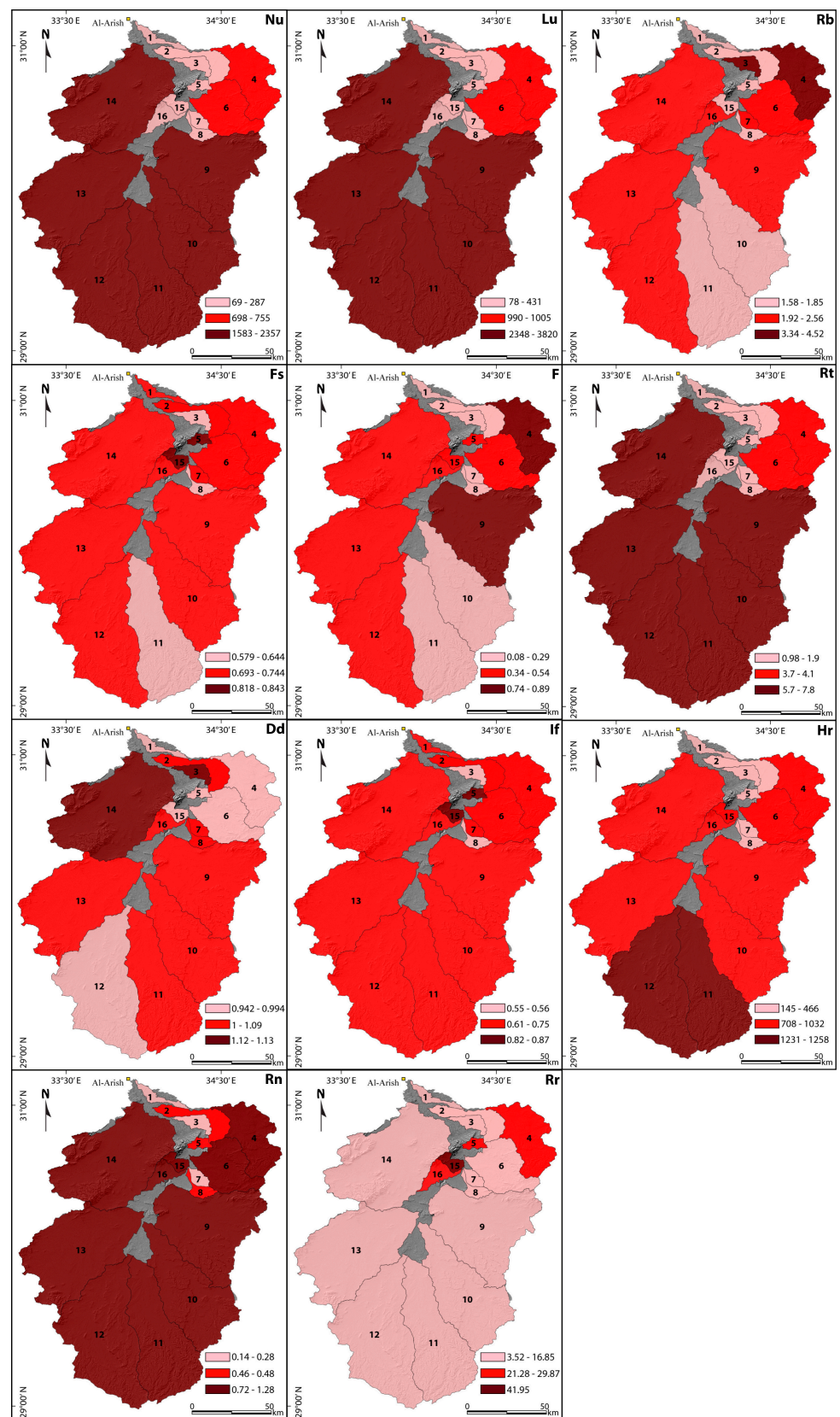


Figure 8. Morpho-metric indices maps; *Nu*: stream number); *Lu*: stream length; *Rb*: bifurcation ratio; *Fs*: stream frequency; *F*: form factor; *Rt*: texture ratio; *Dd*: drainage density; *If*: infiltration number; *Hr*: catchment relief; *Rn*: ruggedness number; and *Rr*: elevation–relief ratio.

Table 3. Stream order (Su) and stream number (Nu) of the proposed catchments.

Catchments	I	II	III	IV	V	VI	Total
C1	51	27	21	0	0	0	99
C2	144	72	37	34	0	0	287
C3	53	24	22	6	0	0	105
C4	380	202	103	19	45	6	755
C5	35	19	8	7	0	0	69
C6	350	168	69	65	39	7	698
C7	38	23	8	6	0	0	75
C8	37	19	9	7	0	0	72
C9	1020	466	276	173	83	18	2036
C10	838	409	207	96	61	60	1672
C11	794	379	223	94	52	41	1583
C12	1167	555	300	195	93	18	2328
C13	1083	510	299	166	63	39	2159
C14	1179	556	323	150	110	38	2357
C15	82	38	31	13	0	0	164
C16	50	27	10	6	5	0	98

4.1.3. Stream Length Index (Lu)

The stream length (Lu) index is recognized as a dimensional index indicating the characteristic size of the water network and its impact on catchment surfaces [40]. It is calculated by dividing the total length of rivers and streams in a given order by the total number of segment lengths in the order. The total stream length of all catchments reaches 216,708.8 m. The stream length values range from 0.789 km (C5) to 38.206 km in catchment 14. The stream length index represents one of the important parameters to measure surface runoff conditions. Long Lu is an indicator of less infiltration and high runoff conditions [43]. The results indicate that consistency with the results comes from the stream number index; the highest and lowest values of them are recorded in C14 and C5, respectively (Table 4 and Figure 8).

Table 4. Calculated values of morpho-metric indices for every single catchment.

Catchments	Nu	Lu	Rb	Fs	F	Rt	Dd	If	Hr	Rn	Rr
C1	99	140.89	1.58	0.69	0.08	0.98	0.99	0.70	145	0.14	03.52
C2	287	431.02	1.67	0.71	0.10	1.91	1.07	0.66	436	0.46	07.12
C3	105	184.65	4.52	0.63	0.18	1.37	1.12	0.56	248	0.27	08.37
C4	755	1005.93	3.43	0.70	0.89	3.75	0.94	0.75	872	0.82	25.27
C5	69	78.93	1.78	0.84	0.41	1.49	0.96	0.87	298	0.28	21.28
C6	698	990.06	2.56	0.69	0.38	4.12	0.98	0.70	858	0.84	16.85
C7	75	110.98	1.95	0.71	0.29	1.61	1.06	0.67	272	0.28	14.31
C8	72	129.37	1.78	0.57	0.15	1.02	1.04	0.55	466	0.48	16.52
C9	2036	2953.69	2.43	0.70	0.74	7.18	1.02	0.68	768	0.78	12.34
C10	1672	2348.20	1.75	0.71	0.25	6.03	1.00	0.71	893	0.89	09.38
C11	1583	2501.54	1.84	0.64	0.22	5.79	1.01	0.63	1258	1.28	12.09
C12	2328	3205.29	2.55	0.71	0.34	7.40	0.98	0.72	1231	1.21	12.70
C13	2159	3413.22	1.97	0.69	0.48	7.15	1.09	0.63	762	0.83	09.46
C14	2357	3820.63	2.05	0.70	0.54	7.82	1.13	0.61	1032	1.17	13.18
C15	164	237.37	1.92	0.74	0.39	1.76	1.07	0.69	708	0.76	29.87
C16	98	119.03	1.58	0.81	0.39	1.81	0.99	0.82	730	0.72	41.95

4.1.4. Bifurcation Ratio Index (Rb)

The bifurcation ratio (Rb) index represents one of the very effective parameters, recognizing the ramification level of the catchment drainage [56]. This index is expressed as a dimensionless index recognizing the ratio of rivers/streams of an examined given order (Nu) to the total number of rivers/streams of the next higher order ($Nu + 1$). Regarding this analysis, the highest values of the bifurcation ratio have been observed for catchments 3, 4, and 12, as 4.52, 3.43, and 2.55, respectively. Subsequently, the lowest values of the Rb are recorded for catchments 1 and 2 as 1.58 and 1.67, respectively (Table 4 and Figure 8). The authors in Refs. [45,46] discussed that, the bifurcation ratio usually provides the highest values over the dissected and mountainous catchments, while providing the lowest values over the rolling or flatness drainage catchments. Therefore, the northeastern area in addition to southern part of the study landscape suggest high conditions of runoff, providing potential associated with low values of lag time for generating floods during heavy rainfall events.

4.1.5. Stream Frequency Index (Fs)

In this analysis, the estimated stream frequency index value for all catchments is 11.3350. The Fs index provides its highest value in catchment 5, covering the northern spot of the study landscape as 0.84, while 0.57 was recorded as a lowest value deriving from this analysis for catchment 8 (Table 4 and Figure 8). The Fs index is commonly used in flood analysis and reveals that high values generally indicate a high volume of runoff transmission, which is a factor of an impervious surface of soils and rocks, high-relief characteristics, and scattered vegetation cover [45,57,58].

4.1.6. Form Factor Index (F)

The form factor (F) index has broadly been used to predict the intensity of the flow of a catchment (e.g., Ref. [59]). The results from this analysis record the highest value for catchment 4 as 0.89 in the northeastern part of the landscape. The F lowest results were calculated for catchment 1 as 0.084 (Table 4 and Figure 8). The authors in Refs. [45,59] applied this index in their research and suggested that the high value of F indicates a high volume of discharge in short duration events, while low F values presents low discharge volumes.

4.1.7. Texture Ratio Index (Rt)

The texture ratio (Rt) index is a factor of climate, slope, rainfall, vegetation, relief, rock, and soil types [45,60]. Regarding this index, soft formations overlaid by vegetation cover and associated with no topographic surface produce fine texture, hard rock reliefs (consolidated formations) generally provide coarse texture [60]. In this study, Rt is categorized into four texture classes: very fine texture ($Rt > 15$ in km), fine texture ($15 > Rt > 10$ in km), moderate texture ($4 < Rt < 10$ in km), and coarse texture ($Rt < 4$ in km) [50]. The Rt index records values between 0.98 and 7.82 for catchments 1 and 14, respectively. Analysis of this index presents values between 4 and 10 for 7 catchments, thus nearly half the catchments reflect intermediate texture and suggest a high peak discharge generation response (see Table 4 and Figure 8). The remaining catchments reveal coarse texture with the lowest values (<4) (see Figure 5 for catchments positions).

4.1.8. Drainage Density Index (Dd)

The drainage density (Dd) index was first recognized and applied by the authors in Refs. [43,46] to describe the drainage catchment characteristics. Authors in References [61,62] introduced Dd as the ratio of the total stream length versus the catchment total area. Authors in Ref. [45] provide a definition of Dd as a total length of all studied orders, which are divided by the total area of the investigated catchment. In the present study, drainage density was recorded to be highest in catchment 14 with a value of 1.13 (Table 4), thus this

catchment is likely producing the highest runoff; whereas catchment 4 provided the lowest Dd value of 0.94 (see Figure 8 for catchments positions).

4.1.9. Infiltration Number Index (If)

With common and recent morpho-hydrological research, the infiltration number (If) index was vastly applied in order to understand the infiltration aspects of different water bodies [45,50]. In this work, the highest values of If are observed for catchment 5 as 0.87, providing a suitable condition for the high rate of infiltration and high amount of runoff [63]. The relatively minimal infiltration characteristics were observed in catchment 8, providing the least infiltration ratio as 0.55 (Table 4 and Figure 8).

4.1.10. Catchment Relief Index (Hr)

The catchment relief (Hr) index helps in effectively in understanding the general rivers denudation, runoff volume, and landform evolution of a studied catchment. The observation analysis from this index states that the highest values of the Hr index were recorded for catchments 11, 14, and 12 as 1258, 11,231, and 1232, respectively (Table 4 and Figure 8). The values extracted from this index are very useful and effective in evaluating the probability degrees of the flooding events. Generally, high values reveal a high level of flood possibility signals, while low values indicate weak conditions for any flash flooding [45].

4.1.11. Ruggedness Number Index (Rn)

The ruggedness number (Rn) index describes the level of slope length and steepness defining the extent of the landscape instability [48,64,65]. Regarding the current work, the Rn index values vary from 0.14 (catchment 1) to 1.28 with catchment 11 (Table 4). A high Rn value usually describes catchments characterized by long and steep slopes, high erosion conditions, and rapid peak flow signals and flash floods [66]. The higher ruggedness numbers were recorded as 1.28, 1.21, and 1.17 for catchment 11, 12, and 14, respectively (see Figure 5 for catchments positions). The previous water bodies show a rugged topography surface, vulnerable to the process of soil corrosion, and are structurally complex. Topographically, Ref. [67] classified landscapes, by Rn , into: badland topography ($Rn > 2$), undulating topography ($1 < Rn < 2$), and flat topography ($Rn < 1$) [45].

4.1.12. Elevation–Relief Ratio Index (Rr)

The Rr index represents one of the common relief aspect parameters, which indicates the topographic characteristics of a catchment [45]. Regarding the analysis of these catchments, values of Rr vary from 3.52 (lowest) for catchment 1 to 41.95 (highest) for catchment 16. The relief ratio index helps in understanding the comparison of relative relief in catchments regardless of variances of topography scale [65] (Table 4 and Figure 8). Thus, higher Rr values indicate low values of lag time, unexpected peak discharge, and high possibility of flood events [57].

4.2. Climatic Changes in Sinai Peninsula

Recently, understanding the general trend of global warming and climatic changes is a vital challenge that helps in defining the direct causes of natural hazards, particularly flood risks [5]. Evidence for rapid climate fluctuation in the Sinai Peninsula was reported based on an analysis of temperatures and rainfall data between 1970 and 2014 [68]. This evidence indicates a decreasing quantity of rainfall and increasing temperatures. The entire Sinai landscape was affected by extreme droughts for many years, but recently has been exposed to sudden heavy rainfall [68].

4.3. Flash Flood Evaluation Based on the General Watershed Level Method

While the general watershed level method has been used to assess different flood hazards in different environmental localities [5,45]; it was applied precisely to investigate

the flash hazard signals in our studied landscape. Based on the different cumulative values calculated from applied methodology, this analysis presents that catchments 1, 9, 11, and 12 describe the highest conditions of discharge volumes, and they are more exposed to heavy flash floods than the other catchments. The catchments are covered over 142.2 km² (C1), 2888.03 km² (C9), 2454.98 km² (C11), 3237.12 km² (C12), which together constitute 41.89% of the total area of the studied landscape (Figure 9). These catchments have been observed to provide a high flash flood susceptibility level. The catchments C4, C6, C7, C10, C13, and C14 constitute a total space of 10,703.08 km² and cover 52.75% of the total study landscape mapped as moderate flash flood level catchments. The low flash flood level signals were recorded for catchments (C2, C3, C5, C8, C15, and C16) providing space present as 9.36%. The results of this method show that the high flash flood susceptibility level catchments, particularly C9, C11, and C12, are highly fractured more than the other catchments. On the other hand, folds recorded in the study landscape prevail over the catchments with moderate levels of flash flood susceptibility (e.g., C13 and C14) (Figure 9). In view of this method, Nekhel–Suder Al Hetan and Nekhel–Taba roads are exposed to high flash flooding signals more than other roads in the study landscape (Figure 9).

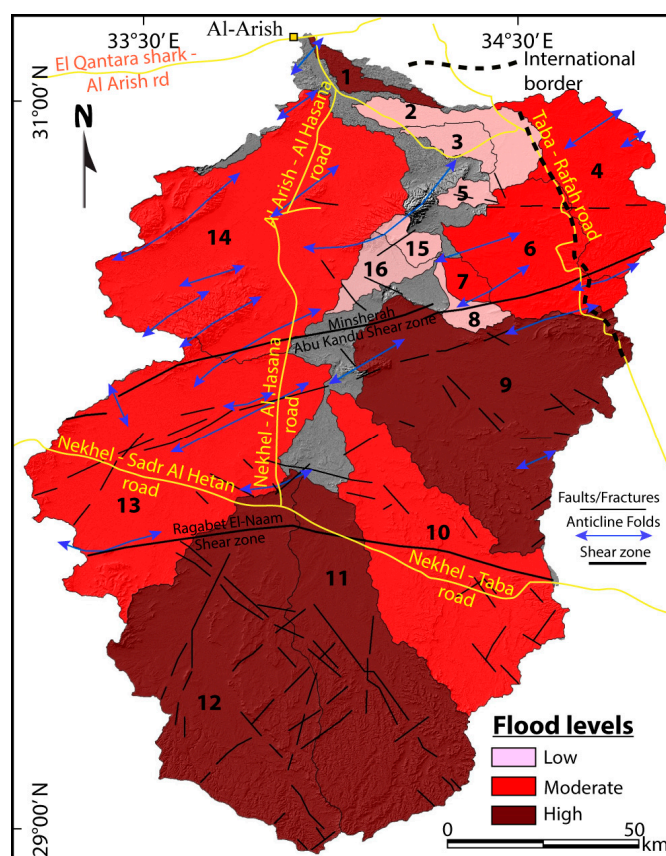


Figure 9. Flash flood levels of the study landscape based on the general watershed method. The gray background is set as a hills-hade base layer.

4.4. Flash Flood Evaluation Based on El-Shamy Method

This method was applied first by the author in Ref. [35] to figure out the relation between flash flood opportunities and the recent recharge of aquifers in arid regions. Based on the analysis of this method, two charts illustrate the bifurcation ratio values from one side against drainage density and stream frequency values, respectively, on the other side. These two quantitative graphs were categorized into three classes of flash flood hazard levels: high level (class B), moderate level (class C), and low level (class A). The relevance of the bifurcation ratio to drainage density presents that five catchments are plotted within class B (C2, C7, C13, C13, C14), while class A (the low class) was constituted by just C3.

Therefore, the rest of the catchments were plotted within class C (Figure 10a). The second chart, which illustrates the bifurcation ratio versus stream frequency, shows that catchments 5, 15, and 16 have a high flood level (class B), while class A is illustrated by catchment 3. In this chart, most of the catchments are presented within field C (Figure 10b). A new detailed hazard level map was extracted from the combination of these charts and presents that the high flood hazard level was recorded for catchments 2, 5, 13, 14, 15, and 16, providing 30% of the total study landscape (Figure 11). The low-level hazard was covered by catchment 3 at just 0.07%, while the moderate level provided spaces as 69.92% for catchments 1, 4, 6, 7, 8, 9, 10, 11, and 12. Results of this method suggest that Al Arish–Al Hasana, Nekhel–Al Hasana, and Nekhel Sadr Al Hetan roads located in the western part of the proposed landscape are highly vulnerable to the heavy flood hazard more than the other roads.

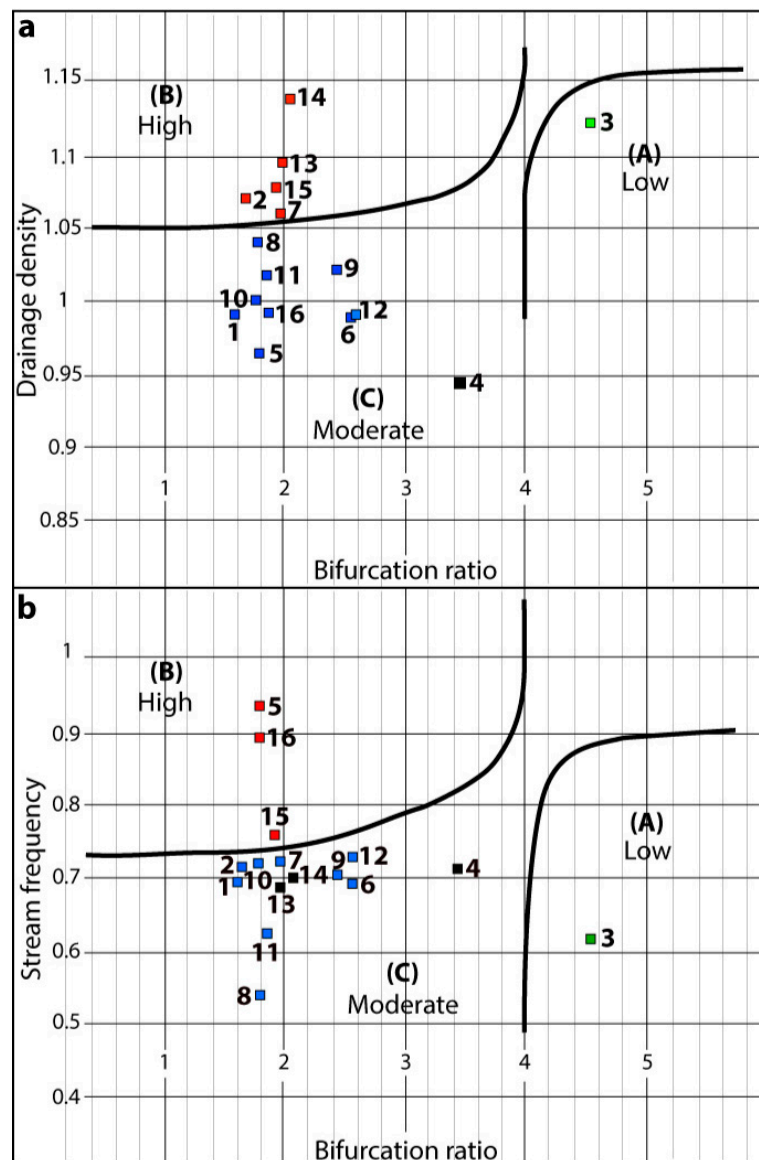


Figure 10. El-Shamy's technique results for evaluating the flood hazard levels; (a) shows the relationship between bifurcation ratio and drainage density and (b) illustrates the relationship between bifurcation ratio and stream frequency.

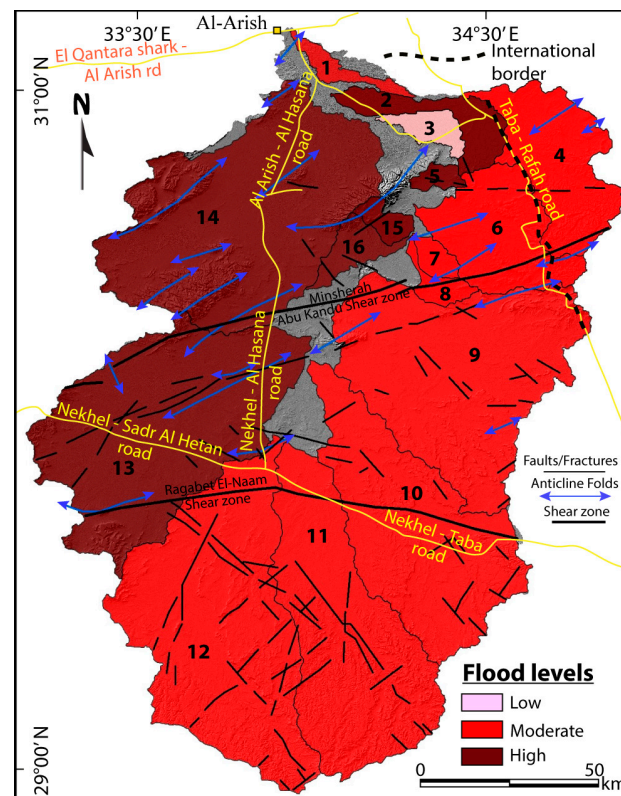


Figure 11. Flash flood susceptibility levels of the study landscape based on the general watershed method. The gray background is set as a hills-hade base layer.

4.5. Flash Flood Evaluation Based on the Ranked Method

The ranked method has been applied vastly and is one of the most common techniques to recognize flood potentialities and evaluate flash flood hazards [37,38]. This method is a linear method equation [38]. It was first applied by the author in Ref. [39] as a new technique of data analysis and statistics in natural hazards. He used this linear equation as a scale to expect the flood risk levels. The ranked method scale in this study was classified into three classes: low class as class 1; moderate class as class 2; and class 3, which indicates the highest flood risk signals. The results from the analysis of this method define high flood level risk for four catchments as C9, C12, C13, and C14. The high flood signals were recorded to cover a space of about 60.47% of the total space of the study landscape (Table 5 and Figure 12). The study observed that the entire western half of the study landscape had high flood level risks, which are characterized by dense fractures and many anticline folds. The eastern half of the investigated landscape is mostly covered by moderate flood level risk catchments (C1: C8, C10, and C11) providing 39.53% of the total landscape space. The results did not show any catchments belonging to the low flood level risks (Table 5 and Figure 12).

Table 5. Flood hazard assessment due to the ranking method.

Catchments	Nu	Lu	Rb	Fs	F	Rt	Dd	If	Hr	Rn	Rr	Sum	General Hazard Level
C1	1.02	1.03	1.00	1.55	1.00	0.99	1.48	1.91	1.00	1.00	0.99	13.02	1.18
C2	1.90	1.18	1.06	1.72	1.05	1.27	2.30	1.68	1.52	1.50	1.17	15.68	1.42
C3	1.03	1.05	3.00	1.00	1.25	1.11	2.84	1.07	1.18	1.21	1.23	16.00	1.45
C4	1.59	1.49	2.26	1.66	2.99	1.80	1.00	2.22	2.30	2.05	2.03	21.45	1.95
C5	1.00	1.00	1.13	3.00	1.82	1.15	1.22	2.99	1.27	1.22	1.84	17.67	1.60
C6	1.54	1.48	1.66	1.56	1.74	1.91	1.47	1.93	2.28	2.10	1.63	19.35	1.75
C7	1.00	1.01	1.24	1.75	1.50	1.18	2.19	1.75	1.22	1.22	1.51	15.62	1.42

Table 5. Cont.

Catchments	Nu	Lu	Rb	Fs	F	Rt	Dd	If	Hr	Rn	Rr	Sum	General Hazard Level
C8	1.00	1.02	1.13	0.41	1.17	1.01	1.99	1.00	1.57	1.53	1.61	13.49	1.22
C9	2.71	2.53	1.57	1.32	2.63	2.81	1.81	1.83	2.11	2.00	1.42	22.78	2.07
C10	2.40	2.21	1.11	1.71	1.43	2.47	1.58	1.97	2.34	2.16	1.72	20.70	1.88
C11	2.32	2.29	1.17	1.05	1.35	2.40	1.77	1.48	3.00	2.77	1.40	21.04	1.91
C12	2.97	2.67	1.47	1.77	1.64	2.87	1.47	2.06	2.95	2.67	1.43	24.21	2.20
C13	2.82	2.78	2.56	1.53	1.97	2.80	2.56	1.47	2.10	2.07	1.28	22.69	2.06
C14	3.00	3.00	3.00	1.62	2.13	3.00	3.00	1.38	2.59	2.61	1.46	25.12	2.28
C15	1.08	1.08	2.37	2.03	1.75	1.22	2.37	1.84	2.01	1.96	2.25	18.86	1.71
C16	1.02	1.02	1.52	2.75	1.76	1.24	1.52	2.67	2.05	1.90	2.83	19.98	1.81

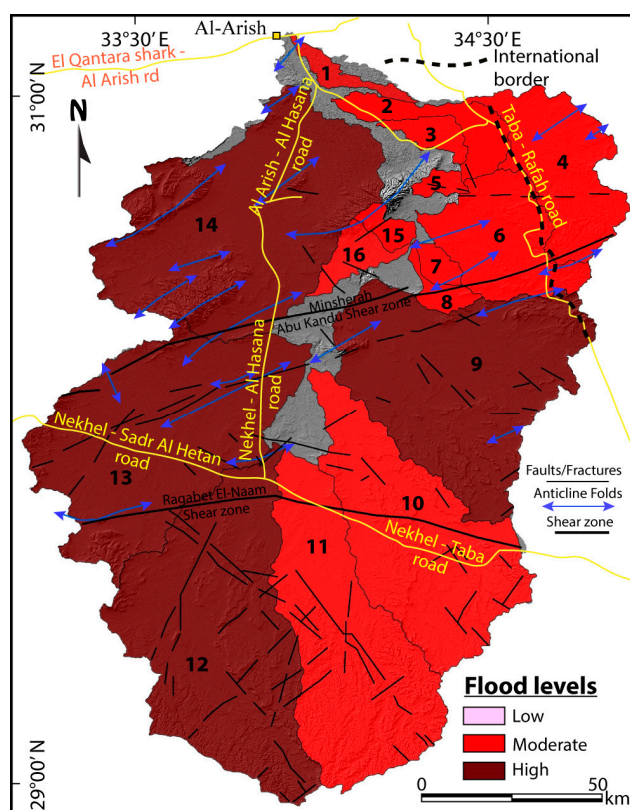


Figure 12. Flash flood levels of the study landscape based on the ranked method. The gray background is set as a hills-hade base layer.

4.6. Overall Evaluation Based on the Combination Methods

The overall comparison between the general watershed method outputs, El-Shamy method plotting, and that of the ranked method results presents that the evaluation according to the general watershed level and El-Shamy methods provide three levels of flash flood hazards, while the ranked method defines only two levels of flood hazards (moderate and high) (Figure 13a). Catchments 4, 6, 7, and 10 provide similar levels of flood hazards through all applied methods as a moderate level, while catchments 2, 5, 14, and 15 present different levels as a low level for the general watershed method, moderate level for the ranked method, and high degree for the El-Shamy method (Figure 13a). The percentage analysis presents that moderate levels prevail through the general watershed and El-Shamy methods (52.75% and 69.92%, respectively), while the high level is observed as higher than the moderate level in the ranked method (Figure 13b). A final detailed map was extracted based on the combination of the applied three methods (Figure 14). A composed index was created for Al-Arish City by the authors in Ref. [69], providing three categories of flood

vulnerability assessments: 13% high vulnerability, 45% moderate vulnerability, and 42% low vulnerability level. The overall evaluation of our paper shows a totally different pattern of flood susceptibilities. They are calculated as 43.33% high level of flood susceptibility, 54.33% moderate flood susceptibility level, and 2.43% low flood susceptibility level. The differences are observed between the high and low levels between the two studies, while the moderate assessment is nearly the same.

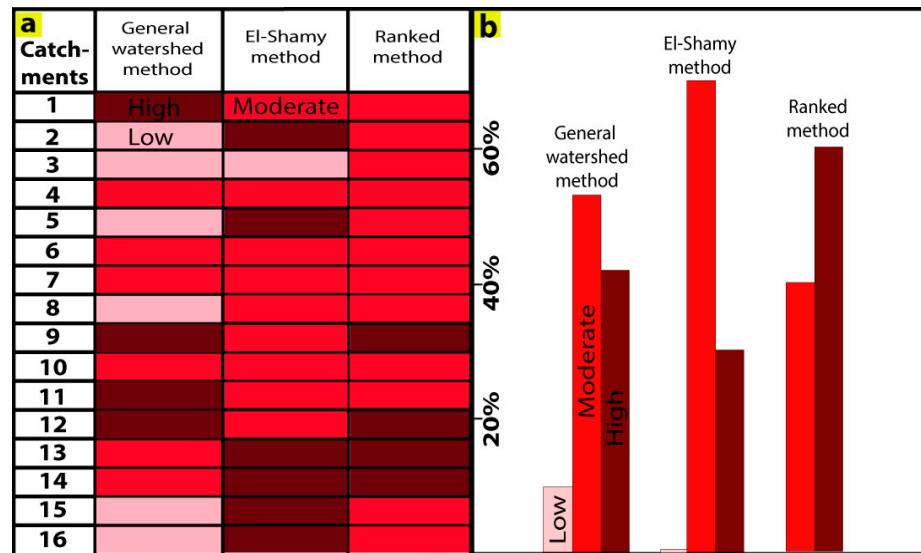


Figure 13. (a) Flash flood levels of all catchments, and (b) flash flood levels percentage through the proposed methods.

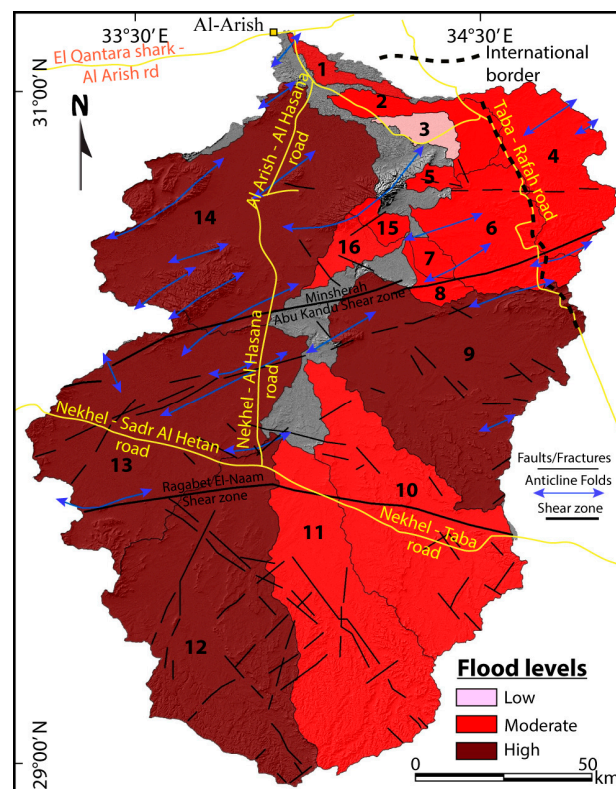


Figure 14. Flood hazard distribution based on the proposed combination method. The gray background is set as a hills-hade base layer.

4.7. Topographic Position Index

The topographic position index (TPI) is a simple and repeatable technique to sort landscapes into slope position and landform categories [45]. It describes the elevation of a cell and the average elevation of the surrounding cells [53]. TPI values aid in identifying various topographic landforms, including different types of slopes, valleys, and topographic ridges [70–72]. In the current paper, TPI processing reflects three different levels of waterlogging probability starting from -48 and ending at 40.8 . The steep mountain edges generally show the lowest potential conditions, causing topographic inundation rather than the areas characterized by low-relief topography. The topographic position index is a very effective parameter to describe the classification of topographic landscape positions, the topographic-driven physical equilibrium of the catchment water, and it provides drainage [73]. TPI positive values provide a higher centric zone than its average neighbors, while negative numbers express lower values than its surroundings (Figure 15). TPI is generally used to identify topographic slopes and automate landscape categorizations [45,74]. In this paper, we applied TPI to recognize the different topographic features including flat plains, depressions, and high-relief ridges. The TPI analysis provides the areas characterized by a high probability of waterlogging. Accordingly, we assume that the impact of the topographic position index is prevailing and effective. Based on this index, the friction of the investigated catchments is assumed to be fully saturated [45,75]. This index can lead to recognizing the topographic structure of the water system, gaining insight into drainage systems, and providing a unique figure of runoff behavior generation [75].

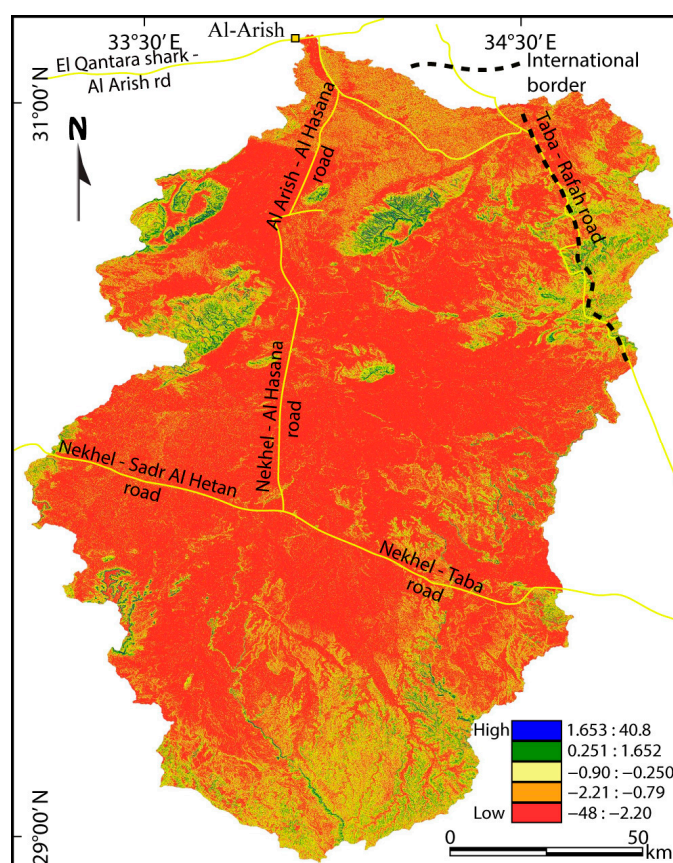


Figure 15. Topographic map of Wadi Al-Arish landscape showing different sites generated by the topographic position index (TPI).

4.8. Flash Flood Hazard Susceptibility Levels

Generally, the dynamic behaviors of sudden environmental events such as flash floods, have never been fully expectable or avoidable. It is highly recommended to improve our

knowledge to investigate the previous events and develop our techniques and methods to build comprehensive models able to precisely forecast future flood events and reduce the negative effects of flash floods. Accordingly, new approaches are required to map flood susceptibility using the most modern and advanced techniques. Three different effective methods were combined in order to obtain objectives and classify the study landscape into different flood-susceptible zones. Every single method was successfully applied to investigate various flash floods [35,45,69], but here we offer this integrated approach to provide important insights into flood event possibilities and proposed area characteristics. Regarding the different cumulative values extracted through the adapted methods, the final analysis suggests that catchments 9, 12, 13, and 14 provide high conditions of discharge-producing potential, and are highly susceptible to flash flooding risks. These catchments are observed over 2888.03 km² (C9), 3237.79 km² (C13), 3111.62 km², and 3351.79 km², which all constitute 60.74% of the total space of the study landscape (Figure 14). Analysis of the morphometric indices through the three cumulative methods presents a moderate level of flash flood susceptibility for catchments 4 (1067.01 km²), 6 (1000.85 km²), 7 (104.69 km²), and 10 (2347.29 km²), which collectively cover 21.71% of the total area. Only these catchments provide similar levels of flood susceptibility through the applied three methods (Figure 13a). The overall analysis shows the different three flood susceptibility levels through the adapted three methods for catchments 15 (220.16 km²) and 16 (119.73 km²). These catchments have been recorded as low flood susceptibility levels based on the general watershed method, moderate levels through the El-Shamy method, and high levels according to the ranked method. Catchment 3 provides a low level of flood susceptibility due to two adapted methods; therefore, this catchment only was mapped as a low-level flood susceptibility catchment (Figures 13a and 14). Combining the catchment level susceptibility final map (Figure 14) in situ with one of the most effective and indicative topographic index (TPI) results (Figure 15), through the processing of weighted overlay step in ArcGIS 10.4 software, allows to accurately define the flash flood susceptibility for every single part (30 m × 30 m pixel) in all the examined watersheds (Figure 16). Regarding tectonic influences, the final detailed map shows dense fractures over catchments 9, 11, 12, and 13 (high-level flood susceptibility catchments), whereas anticline folds prevail over catchments 4, 6, 9, 13, and 14, which are characterized by both conditions of moderate and high flood susceptibility levels. Additionally, the high susceptibility level catchments are crossed by E–W shear zones (Minsherah Abu kandu and Ragabet El-Naam). Thus, we assume that highly fractured regions are more vulnerable to flood risks than other regions. The final analysis of this study suggests that Nrkul-Sadr Al Hetan, Nekhel-Al Hasana, and Al Arish-Al Hasana roads are more exposed to flood hazard signals than the other roads in the study landscape. Based on some climatic change evidence of the Sinai Peninsula in addition to our results, we can claim that, if the general tendency of rapid fluctuation of climate continues, the environmental balance conditions, including the growth of the population of many important plants and animals, will be harmed in Al-Arish city.

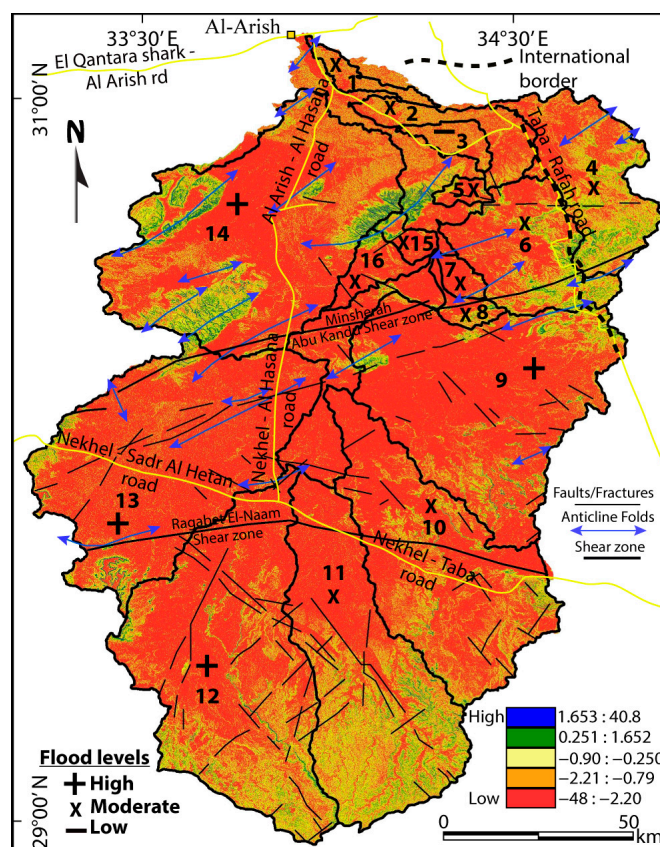


Figure 16. Final flash flood susceptibility scenario of Wadi Al-Arish landscape.

5. Conclusions and Suggestions

Periodically, several locations worldwide are suffering from rainfall-produced floods causing loss of lives, personal injuries, economic injury, and property damage. Investigating the flood potential of the different drainage catchments is highly recommended for minimizing its dangerous effects. In this current study, very useful morpho-metric indices were derived from the digital elevation model dataset using various analysis tools through the ArcGIS 10.4 software. These indices affecting flow velocity, water depth, and runoff volume were evaluated over sixteen different-sized catchments covering the study landscape. Three different quantitative methods named general watershed level method, El-Shamy method, and ranked method were run using these indices to assess and gain a comprehensive understanding of the flash flood hazard behaviors of the Wadi Al-Arish landscape in the northern portion of Sinai in Egypt. The results present that catchments 9, 12, 13, and 14 reflect a high intensity level of flood events and can produce intense and large discharge; these catchments provide conditions of high susceptibility flash flood levels more than the other catchments considered for this study. Catchments 12, 13, and 14 extend along the entire western half of the study landscape, whereas catchment 9 covers a space of the eastern half of the study landscape. These high flood susceptibility level catchments are highly fractured and carry most of the anticline folds that affect the study landscape. Two large horizontal shear zones run across these catchments as well. In addition to the three different methods scales characteristics, providing the effective local topographic index significantly aided in precisely defining and tracing the flood susceptibility signals over all sixteen catchments and presents the uniqueness of this analysis. Moreover, the dataset vertical accuracy applied in this analysis (30 m resolution, SRTM, and RMSE equal to 8.28 m) is a point of discussion that restricts practical adaptation of the extracted values/results at a specific scale, requiring precise information. The flash flood hazard events are not totally a function of morpho-metric characteristics; thus, the scenarios may vary due to the impact of other factors, such as lithology, land use, flood management in each catchment,

and hydraulic structures along the master rivers and channels. Despite this, we do not assign uncertainties to the dataset and applied methods, the outputs of the current work provide valuable understanding of flood behavior and help develop the heavy rainfall mitigation plan for the proposed important landscape. Finally, the current work suggests some guidelines to improve the flood risk assessment and quick response system in the study, which in turn can be applied successfully in other regions with similar conditions. Suggestions are summarized as follows:

1. Focus on applying the most modern advanced methods and data to monitor and evaluate this kind of serious risk preciously;
2. Provide more attention to regularly updating the climatic datasets;
3. Initiate response systems and monitoring stations in order to develop early risks warning techniques;
4. Significant efforts such as hazard communication should be performed to help mitigate flood hazard effects and keep the environment safe and steady.

Author Contributions: Conceptualization, A.K.; methodology, A.K. and S.P.N.; software, A.K., B.B., A.A., S.P.N. and R.N.; validation, A.K., B.B. and A.A.; formal analysis, A.K.; investigation, A.K., B.B. and A.A.; resources, A.K., B.B. and S.P.N.; data curation, A.K., S.P.N. and R.N.; writing—original draft preparation, A.K.; Writing—review and editing, A.K., B.B., A.A., S.P.N. and R.N.; visualization, A.K.; supervision, A.K. and R.N.; project administration, A.K., B.B. and A.A.; funding acquisition, B.B. and A.A. All authors have read and agreed to the published version of the manuscript.

Funding: This research was supported by the Researchers Supporting Project number (RSP2023R296), King Saud University, Riyadh, Saudi Arabia.

Data Availability Statement: Not applicable.

Acknowledgments: The aim, methods, analysis, and results of this paper were discussed, modified, and improved by the structural geology and tectonics lab team of the Department of Geology, Faculty of Science, Al-Azhar University. Most of the processing steps were verified in the remote sensing lab of the Department of Geology, Faculty of Science, Al-Azhar University as well. The authors appreciate the academic editor for handling this work and are thankful to the three reviewers for their positive and constructive comments and suggestions of our manuscript.

Conflicts of Interest: The authors declare no conflict of interest.

References

1. Petrucci, O.; Aceto, L.; Bianchi, C.; Bigot, V.; Brázdil, R.; Pereira, S.; Kahraman, A.; Kılıç, Ö.; Kotroni, V.; Llasat, M.C.; et al. Flood Fatalities in Europe, 1980–2018: Variability, Features, and Lessons to Learn. *Water* **2019**, *11*, 1682. [[CrossRef](#)]
2. Velasco, M.; Versini, P.A.; Cabello, A.; Barrera-Escoda, A. Assessment of flash floods taking into account climate change scenarios in the Llobregat River basin. *Nat. Hazards Earth Syst. Sci.* **2013**, *13*, 3145–3156. [[CrossRef](#)]
3. Khalifa, A.; Bashir, B.; Alsalman, A.; Bachir, H. Morphometric-hydro Characterization of the Coastal Line between El-Qussier and Marsa-Alam, Egypt: Preliminary Flood Risk Signatures. *Appl. Sci.* **2022**, *12*, 6264. [[CrossRef](#)]
4. Dankers, R.; Feyen, L. Flood hazard in Europe in an ensemble of regional climate scenarios. *J. Geophys. Res. Atmos.* **2009**, *114*, 1–16. [[CrossRef](#)]
5. Bashir, B. Morphometric Parameters and Geospatial Analysis for Flash Flood Susceptibility Assessment: A Case Study of Jeddah City along the Red Sea Coast, Saudi Arabia. *Water* **2023**, *15*, 870. [[CrossRef](#)]
6. Dawood, F.; Akhtar, M.M.; Ehsan, M. Evaluating urbanization impact on stressed aquifer of quetta valley, pakistan. *Desalin. Water Treat.* **2021**, *222*, 103–113. [[CrossRef](#)]
7. Suparta, W.; Rahman, R.; Singh, M.S.J. Monitoring the variability of precipitable water vapor over the Klang Valley, Malaysia during flash flood. *IOP Conf. Ser. Earth Environ. Sci.* **2014**, *20*, 012057. [[CrossRef](#)]
8. Bathrellos, G.D.; Karymbalis, E.; Skilodimou, H.D.; Gaki-Papanastassiou, K.; Baltas, E.A. Urban flood hazard assessment in the basin of Athens Metropolitan city, Greece. *Environ. Earth Sci.* **2016**, *75*, 319. [[CrossRef](#)]
9. Alessio, G.; De Falco, M.; Di Crescenzo, G.; Nappi, R.; Santo, A. Flood hazard of the Somma-Vesuvius region based on historical (19–20th century) and geomorphological data. *Ann. Geophys.* **2013**, *56*, S0434. [[CrossRef](#)]
10. Sherwood, J.M. Estimation of Flood Volumes and Simulation of Flood Hydrographs for Ungaged Small Rural Streams in Ohio. *Water-Resour. Investig. Rep.* **1993**, *52*, 4080. [[CrossRef](#)]
11. Dawod, G.M.; Mirza, M.N.; Al-Ghamdi, K.A. GIS-Based Spatial Mapping of Flash Flood Hazard in Makkah City, Saudi Arabia. *J. Geogr. Inf. Syst.* **2011**, *3*, 225–231. [[CrossRef](#)]

12. Manzoor, Z.; Ehsan, M.; Khan, M.B.; Manzoor, A.; Akhter, M.M.; Sohail, M.T.; Hussain, A.; Shafi, A.; Abu-Alam, T.; Abioui, M. Floods and flood management and its socio-economic impact on Pakistan: A review of the empirical literature. *Front. Environ. Sci.* **2022**, *10*, 2480. [[CrossRef](#)]
13. Sohail, M.T.; Hussain, A.; Ehsan, M.; Al-Ansari, N.; Akhter, M.M.; Manzoor, Z.; Elbeltagi, A. Groundwater budgeting of Nari and Gaj formations and groundwater mapping of Karachi, Pakistan. *Appl. Water Sci.* **2022**, *12*, 267. [[CrossRef](#)]
14. Ahmad, N.; Khan, S.; Ehsan, M.; Rehman, F.U.; Al-Shuhail, A. Estimating the Total Volume of Running Water Bodies Using Geographic Information System (GIS): A Case Study of Peshawar Basin (Pakistan). *Sustainability* **2022**, *14*, 3754; Correction in *Sustainability* **2022**, *14*, 8750. [[CrossRef](#)]
15. Li, Z.; Zhang, Y.; Wang, J.; Ge, W.; Li, W.; Song, H.; Guo, X.; Wang, T.; Jiao, Y. Impact evaluation of geomorphic changes caused by extreme floods on inundation area considering geomorphic variations and land use types. *Sci. Total Environ.* **2021**, *754*, 142424. [[CrossRef](#)]
16. Vincent, L.T.; Eaton, B.C.; Leenman, A.S.; Jakob, M. Secondary Geomorphic Processes and Their Influence on Alluvial Fan Morphology, Channel Behavior and Flood Hazards. *J. Geophys. Res. Earth Surf.* **2022**, *127*, e2021JF006371. [[CrossRef](#)]
17. Khalifa, A.; Bashir, B.; Alsaman, A.; Ögretmen, N. Morpho-Tectonic Assessment of the Abu-Dabbab Area, Eastern Desert, Egypt: Insights from Remote Sensing and Geospatial Analysis. *ISPRS Int. J. Geo-Inf.* **2021**, *10*, 784. [[CrossRef](#)]
18. Shah, S.M.H.; Mustaffa, Z.; Teo, F.Y.; Imam, M.A.H.; Yusof, K.W.; Al-Qadami, E.H.H. A review of the flood hazard and risk management in the South Asian Region, particularly Pakistan. *Sci. Afr.* **2020**, *10*, e00651. [[CrossRef](#)]
19. Tariq, M.A.U.R.; Van de Giesen, N. Floods and flood management in Pakistan. *Phys. Chem. Earth* **2012**, *47*, 11–20. [[CrossRef](#)]
20. Ahmad, F.; Kazmi, S.F.; Pervez, T. Human response to hydro-meteorological disasters: A case study of the 2010 flash floods in Pakistan. *J. Geogr. Reg. Plan.* **2011**, *4*, 518–524.
21. Lepesteur, M.; Wegner, A.; Moore, S.A.; McComb, A. Importance of public information and perception for managing recreational activities in the Peel-Harvey estuary, Western Australia. *J. Environ. Manag.* **2008**, *87*, 389–395. [[CrossRef](#)] [[PubMed](#)]
22. Ali, A.; Rana, I.A.; Ali, A.; Najam, F.A. Flood risk perception and communication: The role of hazard proximity. *J. Environ. Manag.* **2022**, *316*, 115309. [[CrossRef](#)] [[PubMed](#)]
23. Ullah, F.; Saqib, S.E.; Ahmad, M.M.; Fadlallah, M.A. Flood risk perception and its determinants among rural households in two communities in Khyber Pakhtunkhwa, Pakistan. *Nat. Hazards* **2020**, *104*, 225–247. [[CrossRef](#)]
24. Jamshed, A.; Birkmann, J.; McMillan, J.M.; Rana, I.A.; Feldmeyer, D.; Sauter, H. How do rural-urban linkages change after an extreme flood event? Empirical evidence from rural communities in Pakistan. *Sci. Total Environ.* **2021**, *750*, 141462. [[CrossRef](#)] [[PubMed](#)]
25. Moawad, M.B. Analysis of the flash flood occurred on 18 January 2010 in wadi El Arish, Egypt (a case study). *Geomat. Nat. Hazards Risk* **2013**, *4*, 254–274. [[CrossRef](#)]
26. Kader, H.A. GIS Based Morphometric Analysis of Wadi el-Arish Watershed Sinai, Egypt-Using ASTER (DEM) Data. *Int. J. Sci. Eng. Res.* **2020**, *11*, 682–694.
27. Elbarbary, S.; Araffa, S.A.S.; El-Shahat, A.; Abdel Zaher, M.; Khedher, K.M. Delineation of water potentiality areas at Wadi El-Arish, Sinai, Egypt, using hydrological and geophysical techniques. *J. Afr. Earth Sci.* **2021**, *174*, 104056. [[CrossRef](#)]
28. Bakheet, A.; Sefelnasr, A. Application of Remote Sensing data (GSMaP) to Flash Flood Modeling in an Arid Environment, Egypt. *Int. Conf. Chem. Environ. Eng.* **2018**, *9*, 252–272. [[CrossRef](#)]
29. Morad, N. Assessment of the Rainfall Storm Events of January 2010 and March 2014 for the Catchment Modeling of Wadi El Arish and Wadi Wardan Basins, Sinai, Egypt. *Egypt. J. Desert Res.* **2016**, *66*, 137–168. [[CrossRef](#)]
30. General Petroleum Corporation. *Geological Map of Egypt, Scale 1:500,000*; Gebel Hamata: Cairo, Egypt, 1987.
31. Abdelsalam, M.G.; Stern, R.J. Sutures and shear zones in the Arabian-Nubian shield. *J. Afr. Earth Sci.* **1996**, *23*, 289–310. [[CrossRef](#)]
32. Moustafa, A.R. Structural setting and tectonic evolution of North Sinai folds, Egypt. *Geol. Soc. Spec. Publ.* **2010**, *341*, 37–63. [[CrossRef](#)]
33. Abdelfadil, K.M.; Obeid, M.A.; Azer, M.K.; Asimow, P.D. Late Neoproterozoic adakitic lavas in the Arabian-Nubian shield, Sinai Peninsula, Egypt. *J. Asian Earth Sci.* **2018**, *158*, 301–323. [[CrossRef](#)]
34. El-Ghazawi, M.M. Hydrogeological Studies in Northeast Sinai, Egypt. Ph.D. Thesis, Departement of Geology, Faculty of Science, Mansoura University, Mansoura, Egypt, 1989; 290p.
35. El-Shamy, I. Recent Recharge and Flash Flooding Opportunities in the Eastern Desert, Egypt. *Annals of Geological Survey of Egypt*. *Ann. Geol. Surv. Egypt* **1992**, *18*, 323–334.
36. Bajabaa, S.; Masoud, M.; Al-Amri, N. Flash flood hazard mapping based on quantitative hydrology, geomorphology and GIS techniques (case study of Wadi Al Lith, Saudi Arabia). *Arab. J. Geosci.* **2014**, *7*, 2469–2481. [[CrossRef](#)]
37. Elsadek, W.M.; Ibrahim, M.G.; Mahmud, W.E.; Kanae, S. Developing an overall assessment map for flood hazard on large area watershed using multi-method approach: Case study of Wadi Qena watershed, Egypt. *Nat. Hazards* **2019**, *95*, 739–767. [[CrossRef](#)]
38. Kamel, M.; Arfa, M. Integration of remotely sensed and seismicity data for geo-natural hazard assessment along the Red Sea Coast, Egypt. *Arab. J. Geosci.* **2020**, *13*, 1195. [[CrossRef](#)]
39. Davis, J.C. *Statistics and Data Analysis in Geology*, 3rd ed.; Wiley: New York, NY, USA, 1975; 656p.
40. Horton, R.E. Erosional development of streams and their drainage basins: Hydrophysical approach to quantitative morphology. *Bull. Geol. Soc. Am.* **1945**, *56*, 275–370. [[CrossRef](#)]

41. Cotti, D.; Harb, M.; Hadri, A.; Aboufirass, M.; Chaham, K.R.; Libertino, A.; Campo, L.; Trasforini, E.; Krätzschar, E.; Bellert, F.; et al. An Integrated Multi-Risk Assessment for Floods and Drought in the Marrakech-Safi Region (Morocco). *Front. Water* **2022**, *4*, 886648. [[CrossRef](#)]
42. Owen, L.A. 5.2 Tectonic Geomorphology: A Perspective. In *Treatise on Geomorphology*; Elsevier: Amsterdam, The Netherlands, 2013; Volume 148, pp. 3–12, ISBN 9780123983534.
43. Horton, R.E. Drainage-basin characteristics. *Trans. Am. Geophys. Union* **1932**, *13*, 350–361. [[CrossRef](#)]
44. Arnous, M.O.; Aboulela, H.A.; Green, D.R. Geo-environmental hazards assessment of the north western Gulf of Suez, Egypt. *J. Coast. Conserv.* **2011**, *15*, 37–50. [[CrossRef](#)]
45. Alam, A.; Ahmed, B.; Sammonds, P. Flash flood susceptibility assessment using the parameters of drainage basin morphometry in SE Bangladesh. *Quat. Int.* **2021**, *575–576*, 295–307. [[CrossRef](#)]
46. Horton, R.E.; Hiltrata, T. Erosional development of streams and their drainage basins, hydrophysical approach to quantitative morphology. *J. Jpn. For. Soc.* **1955**, *37*, 417–420. [[CrossRef](#)]
47. Schumm, S.A. Evolution of drainage systems and slopes in badlands at Perth Amboy, New Jersey. *Geol. Soc. Am. Bull.* **1956**, *67*, 597–646. [[CrossRef](#)]
48. Strahler, A. Dynamic Basis of Geomorphology. *Geol. Soc. Am. Bull.* **1952**, *63*, 923–938. [[CrossRef](#)]
49. El-Fakharany, M.A.; Mansour, N.M. Morphometric analysis and flash floods hazards assessment for Wadi Al Aawag drainage Basins, southwest Sinai, Egypt. *Environ. Earth Sci.* **2021**, *80*, 168. [[CrossRef](#)]
50. Smith, K.G. Standards for grading texture of erosional topography. *Am. J. Sci.* **1950**, *248*, 655–668. [[CrossRef](#)]
51. Faniran, A. The Index of Drainage Intensity—A Provisional New Drainage Factor. *Aust. J. Sci.* **1968**, *31*, 328–330.
52. Melton, M.A. *An Analysis of the Relations Among Elements of Climate, Surface Properties, and Geomorphology*; Technical Report 11; Office of Naval Research, Geography Branch: New York, NY, USA, 1957; 102p. [[CrossRef](#)]
53. Weiss, A. Topographic position and landforms analysis. In Proceedings of the Poster Presentation, ESRI User Conference, San Diego, CA, USA, 9–13 July 2001.
54. Strahler, A.N. Quantitative Geomorphology of Drainage Basins and Channel Networks. In *Handbook of Applied Hydrology*; Chow, V.T., Ed.; McGraw Hill B. Company: New York, NY, USA, 1964; pp. 439–476.
55. Bhat, M.S.; Alam, A.; Ahmad, S.; Farooq, H.; Ahmad, B. Flood hazard assessment of upper Jhelum basin using morphometric parameters. *Environ. Earth Sci.* **2019**, *78*, 54. [[CrossRef](#)]
56. Mesa, L.M. Morphometric analysis of a subtropical Andean basin (Tucumán, Argentina). *Environ. Geol.* **2006**, *50*, 1235–1242. [[CrossRef](#)]
57. Patton, P.C. Drainage basin morphometry and floods. In *Flood Geomorphology*; Baker, V., Kochel, R., Patton, P., Eds.; Wiley: New York, NY, USA, 1988; pp. 51–65.
58. Obi Reddy, G.P.; Maji, A.K.; Gajbhiye, K.S. Drainage morphometry and its influence on landform characteristics in a basaltic terrain, Central India—A remote sensing and GIS approach. *Int. J. Appl. Earth Obs. Geoinf.* **2004**, *6*, 1–16. [[CrossRef](#)]
59. Gregory, K.J.; Wallingford, D.E. *Drainage Basin Form and Process—A Geomorphological Approach*; Wiley: New York, NY, USA, 1973; 456p. [[CrossRef](#)]
60. Hajam, R.A.; Hamid, A.; Bhat, S. Application of Morphometric Analysis for Geo-Hydrological Studies Using Geo-Spatial Technology—A Case Study of Vishav Drainage Basin. *J. Waste Water Treat. Anal.* **2013**, *4*, 1–12. [[CrossRef](#)]
61. Azor, A.; Keller, E.A.; Yeats, R.S. Geomorphic indicators of active fold growth: South Mountain-Oak Ridge anticline, Ventura basin, southern California. *Bull. Geol. Soc. Am.* **2002**, *114*, 745–753. [[CrossRef](#)]
62. Keller, E.A.; Pinter, N. *Active Tectonics: Earthquakes, Uplift and Landscape*, 2nd ed.; Prentice Hall: Upper Saddle River, NJ, USA, 2002.
63. Bhatt, S.; Ahmed, S.A. Morphometric analysis to determine floods in the Upper Krishna basin using Cartosat DEM. *Geocarto Int.* **2014**, *29*, 878–894. [[CrossRef](#)]
64. Kabite, G.; Gessesse, B. Hydro-geomorphological characterization of Dhidhessa River Basin, Ethiopia. *Int. Soil Water Conserv. Res.* **2018**, *6*, 175–183. [[CrossRef](#)]
65. Costa, J.E. Hydraulics and basin morphometry of the largest flash floods in the conterminous United States. *J. Hydrol.* **1987**, *93*, 313–338. [[CrossRef](#)]
66. Patton, P.C.; Baker, V.R. Morphometry and floods in small drainage basins subject to diverse hydrogeomorphic controls. *Water Resour. Res.* **1976**, *12*, 941–952. [[CrossRef](#)]
67. Adnan, M.S.G.; Dewan, A.; Zannat, K.E.; Abdullah, A.Y.M. The use of watershed geomorphic data in flash flood susceptibility zoning: A case study of the Karnaphuli and Sangu river basins of Bangladesh. *Nat. Hazards* **2019**, *99*, 425–448. [[CrossRef](#)]
68. Dadamouny, M.A.; Schnittler, M. Trends of climate with rapid change in Sinai, Egypt. *J. Water Clim. Chang.* **2016**, *7*, 393–414. [[CrossRef](#)]
69. Mohamed, S.A.; El-Raey, M.E. Vulnerability assessment for flash floods using GIS spatial modeling and remotely sensed data in El-Arish City, North Sinai, Egypt. *Nat. Hazards* **2020**, *102*, 707–728. [[CrossRef](#)]
70. Pawluszek, K.; Borkowski, A. Impact of DEM-derived factors and analytical hierarchy process on landslide susceptibility mapping in the region of Rożnów Lake, Poland. *Nat. Hazards* **2017**, *86*, 919–952. [[CrossRef](#)]
71. Jebur, M.N.; Pradhan, B.; Tehrany, M.S. Optimization of landslide conditioning factors using very high-resolution airborne laser scanning (LiDAR) data at catchment scale. *Remote Sens. Environ.* **2014**, *152*, 150–165. [[CrossRef](#)]

72. Pourghasemi, H.R.; Moradi, H.R.; Fatemi Aghda, S.M.; Gokceoglu, C.; Pradhan, B. GIS-based landslide susceptibility mapping with probabilistic likelihood ratio and spatial multi-criteria evaluation models (North of Tehran, Iran). *Arab. J. Geosci.* **2014**, *7*, 1857–1878. [[CrossRef](#)]
73. Görüm, T. Tectonic, topographic and rock-type influences on large landslides at the northern margin of the Anatolian Plateau. *Landslides* **2019**, *16*, 333–346. [[CrossRef](#)]
74. De Reu, J.; Bourgeois, J.; Bats, M.; Zwertvaegher, A.; Gelorini, V.; De Smedt, P.; Chu, W.; Antrop, M.; De Maeyer, P.; Finke, P.; et al. Application of the topographic position index to heterogeneous landscapes. *Geomorphology* **2013**, *186*, 39–49. [[CrossRef](#)]
75. Woods, R.A.; Sivapalan, M. A connection between topographically driven runoff generation and channel network structure. *Water Resour. Res.* **1997**, *33*, 2939–2950. [[CrossRef](#)]

Disclaimer/Publisher’s Note: The statements, opinions and data contained in all publications are solely those of the individual author(s) and contributor(s) and not of MDPI and/or the editor(s). MDPI and/or the editor(s) disclaim responsibility for any injury to people or property resulting from any ideas, methods, instructions or products referred to in the content.